iScience

CellPress
OPEN ACCESS

Article

A mechanism of cooling hot tumors: Lactate attenuates inflammation in dendritic cells

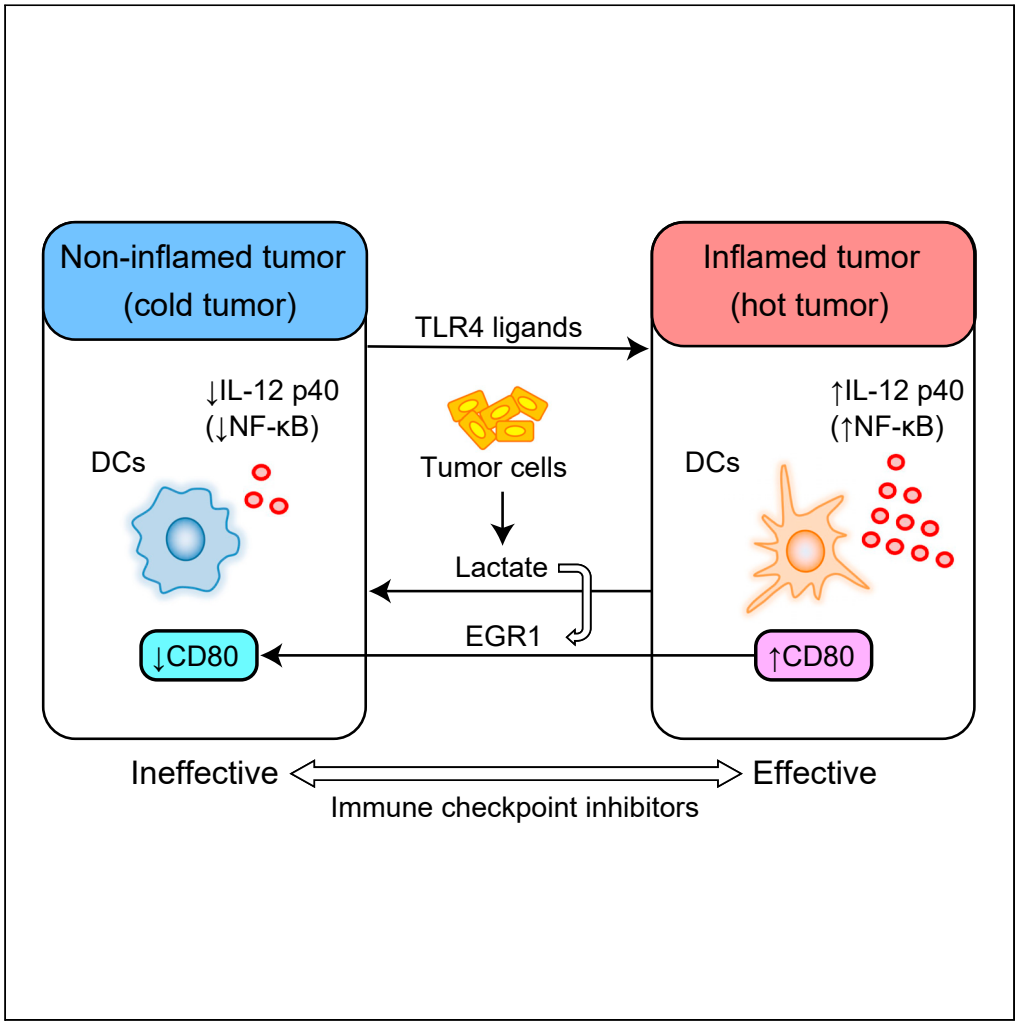

Hisashi Kanemaru, Yukari Mizukami, Akira Kaneko, ..., Shinichi Masuguchi, Satoshi Fukushima, Hironobu Ihn

hisashikanemaru@gmail.com

Highlights

Lactate suppressed IL-12 p40 expression in dendritic cells

Lactate promoted the expression of early growth response protein 1 (EGR1)

EGR1 interacts with serum response factor (SRF) and represses the expression of CD80

Lactate and EGR1 switch inflamed (hot) tumors to non-inflamed (cold) tumors

Kanemaru et al., iScience *24*, 103067
September 24, 2021
https://doi.org/10.1016/j.isci.2021.103067

iScience

CellPress
OPEN ACCESS

Article

A mechanism of cooling hot tumors: Lactate attenuates inflammation in dendritic cells

Hisashi Kanemaru,[1,2,*] Yukari Mizukami,[1] Akira Kaneko,[1] Hidemi Tagawa,[1] Toshihiro Kimura,[1] Haruka Kuriyama,[1] Soichiro Sawamura,[1] Ikko Kajihara,[1] Katsunari Makino,[1] Azusa Miyashita,[1] Jun Aoi,[1] Takamitsu Makino,[1] Shinichi Masuguchi,[1] Satoshi Fukushima,[1] and Hironobu Ihn[1]

SUMMARY

Turning non-inflamed (cold) tumors into inflamed (hot) tumors is important for maximizing the effect of immune checkpoint inhibitors (ICIs) against malignancies. We showed that lactate, a product of the Warburg effect, inhibited the efficacy of ICIs and suppressed IL-12 p40 expression in dendritic cells (DCs) through reducing NF-κB p65, p50, and c-Rel DNA-binding activity to the IL-12 p40 promoter. Additionally, lactate promoted the expression of early growth response protein 1 (EGR1), whose expression was increased in human invasive melanoma compared with non-invasive melanoma. We also found that EGR1 interacts with serum response factor (SRF) and represses the expression of CD80 in DCs. These findings suggest that lactate and its induced EGR1 are key factors that turn hot tumors into cold tumors and may represent targets in cancer treatment with ICIs.

INTRODUCTION

Malignant neoplasms are life-threatening diseases for which effective treatments are urgently needed. Immune checkpoint inhibitors (ICIs) have recently proven to be effective against tumors, demonstrating that the immune system plays a critical role in suppressing malignancies. However, the therapeutic responses to ICIs vary considerably among individual patients; therefore, elucidation of their mechanisms is required to design strategies for improving their therapeutic efficacy (Chen and Mellman, 2017). One important factor that determines the effectiveness of ICIs may be inflammation of the tumor environment. ICIs are effective against inflamed tumors, so-called "hot tumors," in which many pro-inflammatory cytokines are detected (Herbst et al., 2014). Conversely, non-inflamed tumors, so-called "cold tumors," have no tumor-suppressive cytokines or co-stimulators of antigen-presenting cells and rarely respond to ICIs (Herbst et al., 2014). Because dendritic cells (DCs) secrete various cytokines and also have antigen-presenting ability, they may be key regulators in ICI treatment and greatly affect treatment effectiveness (Chen and Mellman, 2017).

Recently, tumor-derived metabolites were reported to have an important effect on immune cells (O'Neill et al., 2016). Lactate accumulation in the tumor environment occurs as a result of the accelerated glucose metabolism in tumor cells, the so-called Warburg effect (Brand et al., 2016). Accumulation of lactate in solid tumors is a pivotal step in the development of malignancies (Hirschhaeuser et al., 2011). In human primary tumors, high levels of lactate correlate with the incidence of distant metastases (Walenta et al., 2000). Recent studies have suggested that the tumor-promoting effect of lactate is related to its immunosuppressive effect within the tumor environment (Brand et al., 2016). For example, one study reported that tumor-derived lactate inhibits the activation and differentiation of T cells and monocytes *in vitro* (Dietl et al., 2010; Fischer et al., 2007) and promotes the development of immunosuppressive M2-like macrophages (Colegio et al., 2014). Yang et al. (Yang et al., 2020) reported that lactate suppresses the macrophage pro-inflammatory response to LPS stimulation by inhibition of YAP and NF-κB activation via GPR81-mediated signaling. Gottfried et al. (Gottfried et al., 2006) reported that lactate inhibits DC activation during antigen-specific T cell stimulation. Other studies reported that lactate skews DC differentiation into a tolerogenic phenotype, as exemplified by increased production of IL-10 and loss of IL-12 (Dong and Bullock, 2014; Nasi et al., 2013). Another report showed that lactate attenuates IFNα induction and induces pro-tumor

[1]Department of Dermatology and Plastic Surgery, Faculty of Life Sciences, Kumamoto University, 1-1-1 Honjo, Kumamoto, Japan

[2]Lead contact

*Correspondence: hisashikanemaru@gmail.com

https://doi.org/10.1016/j.isci.2021.103067

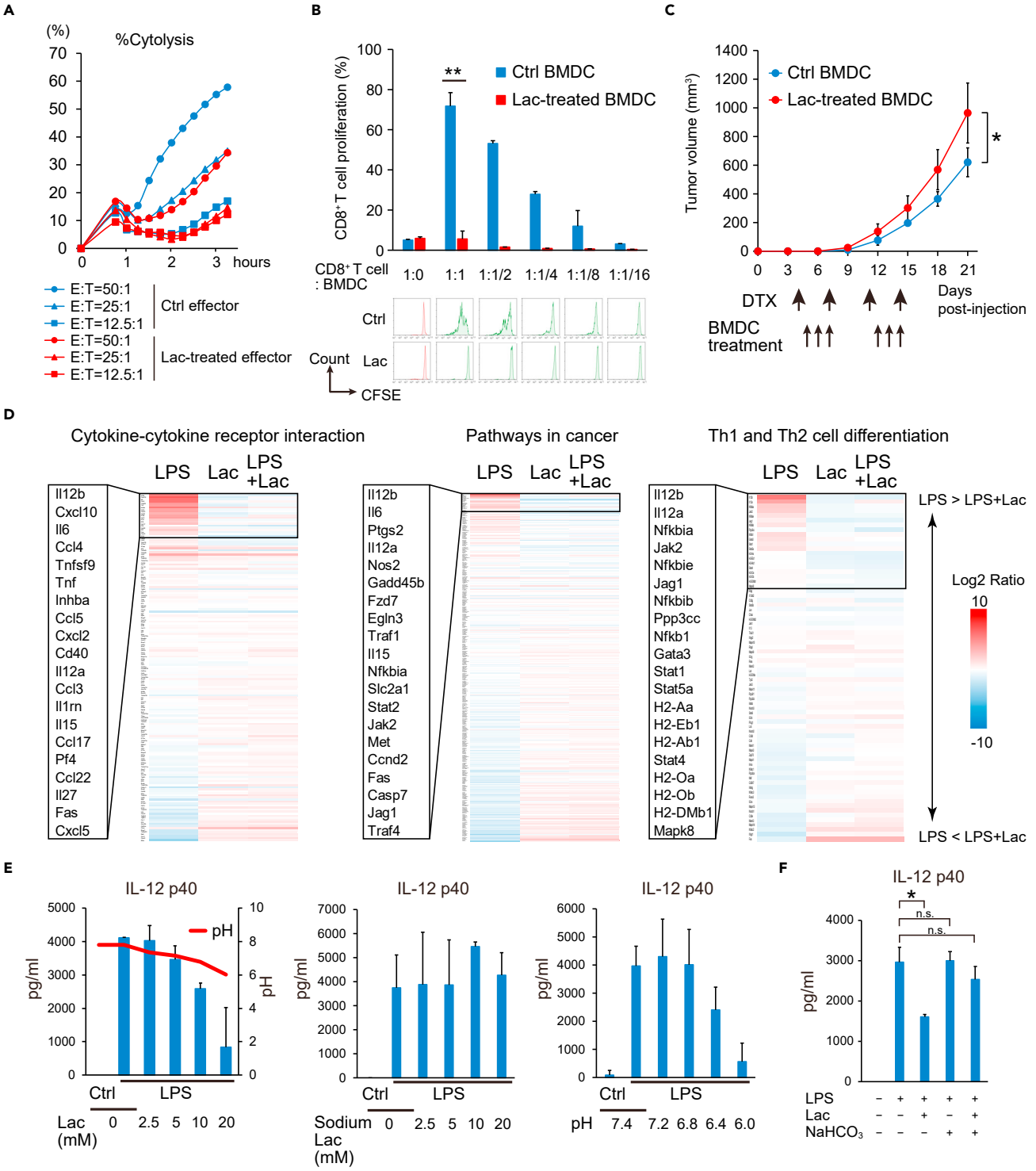

Figure 1. Lactate (Lac) attenuates the antigen-presenting ability of dendritic cells (DCs) and suppresses IL-12 p40 expression in DCs

(A) Cytotoxicity of Lac-treated (20 mM) cytotoxic T lymphocytes (CTLs) and control CTLs against B16-F1 target cells at the indicated effector:target (E:T, CTL:B16-F1 cell) ratios. %Cytolysis was determined by the xCELLigence system.

(B) Carboxyfluorescein succinimidyl ester (CFSE)-labeled $CD8^+$ T cells from OT-I transgenic mice and Lac-treated (20 mM) bone marrow-derived DCs (BMDCs) or control BMDCs from WT mice pulsed with Ova 257–264 peptide were co-cultured at decreasing dilutions ($CD8^+$ T cell:BMDC = 1:1–1:1/16). Proliferation of $CD8^+$ T cells was assessed after 84 hr by flow cytometry (top graph). Representative plots are shown (bottom panels).

Figure 1. *Continued*

(C) Tumor growth kinetics in diphtheria toxin (DTX)-treated CD11c-DTR bone marrow chimeric mice with subcutaneous injection with 1 × 10^6 B16-F1 melanoma cells and treated intratumorally with Lac (5 mM) or PBS-treated BMDCs (1×10^6) as indicated. Data are shown as mean ± SD (n = 4 mice per group).

(D) BMDCs from WT mice were stimulated with LPS (100 ng/mL) and/or Lac (20 mM) for 4 hr, and the total RNA from these cells was subjected to microarray analysis. The log2 ratio for each of the corresponding genes in BMDCs stimulated with LPS was subtracted from that of BMDCs stimulated with LPS plus Lac, and the results were arranged in descending order. Genes categorized in the indicated Kyoto Encyclopedia of Genes and Genomes pathways were analyzed. The top 20 most highly differentially expressed genes are indicated in the box.

(E) Levels of IL-12 p40 secreted by BMDCs following stimulation by LPS and/or indicated concentrations of Lac or sodium Lac for 24 hr were measured by ELISA (left and center). pH levels at the indicated Lac concentrations are also shown. Levels of IL-12 p40 secreted by BMDCs under the indicated pH (adjusted by HCl) are also shown (right).

(F) Levels of IL-12 p40 secreted by BMDCs following stimulation by LPS (100 ng/mL) Lac (20 mM), and/or $NaHCO_3$ for 24 hr were measured by ELISA.

Data are expressed as mean ± SD. Significance was analyzed using a two-tailed Student's t-test, Welch's t test, or Mann-Whitney's U test. *$p < 0.05$; **$p < 0.01$; n.s., not significant ($p > 0.05$). Ctrl: control. See also Figures S1–S6.

reprogramming in plasmacytoid DCs (Raychaudhuri et al., 2019). These results suggest the possible inhibitory effect of tumor-derived lactate on DCs and the therapeutic activity of ICIs, which may represent key factors to determine the hot or cold status of a tumor. Here, we focused on lactate and examined its effect on tumor immunity and particularly its effect on DCs.

RESULTS

Lactate suppresses IL-12 p40 expression in DCs and promotes tumor growth in a mouse model

To investigate the *in vitro* effects of lactate on cytotoxicity of cytotoxic T lymphocyte (CTLs) against tumor cells, we performed a CTL killing assay using the xCELLigence system (Figure S1). We found that lactate treatment attenuated the cytotoxicity of CTLs against B16-F1 cells (Figure 1A). We also performed antigen-presentation assays with OT-I transgenic mouse cells and observed markedly reduced proliferation in OT-I $CD8^+$ cells cultured with bone marrow-derived DCs (BMDCs) stimulated by lactate compared with control cells (Figure 1B), which suggests the attenuation of the antigen-presenting ability of lactate-treated DCs. To examine whether lactate induced apoptosis of effector cells and BMDCs, we evaluated apoptosis using the Annexin V/Propidium Iodide apoptosis assay. The ratio of Annexin V^+ PI^+ apoptotic cells was similar in effector cells and BMDCs stimulated with 0–20 mM lactate (Figure S2), which is consistent with the previous report (Yang et al., 2020).

These results prompted us to investigate the effects of lactate on DCs. To investigate the *in vivo* effects of lactate on DCs, we established a tumor mouse model using DC-depleted mice by subcutaneously injecting mice with B16-F1 melanoma cells. After CD11c-DTR bone marrow chimeric mice were treated with diphtheria toxin and DCs were depleted, mice were subcutaneously injected with lactate-treated (5 mM) BMDCs or non-treated control BMDCs. Increased tumor growth was observed in the mice injected with lactate-treated BMDCs compared with mice injected with control BMDCs (Figure 1C). In addition, increased tumor growth was observed in the mice treated with lactate (5 mM) compared with controls, and the anti-tumor efficacy of anti-PD-L1 was reduced in the lactate treatment group compared with the mice treated with PBS (Figure S3).

Because TLR4 agonists are one of the damage-associated molecular patterns, which are important stimulators of DCs in the tumor microenvironment, we assessed the effects of lactate on the response to LPS, the TLR4 ligand. We performed microarray analyses using BMDCs from WT mice that had been stimulated with LPS, lactate, or LPS together with lactate. Within several Kyoto Encyclopedia of Genes and Genomes (KEGG) categories, such as the cytokine-cytokine receptor interaction, pathways in cancer, Th1 and Th2 cell differentiation, and Toll-like receptor signaling pathway, the *Il12b* gene was the most differentially expressed gene in BMDCs stimulated with LPS and lactate compared those stimulated with LPS (Figures 1D and S4). We further found that lactate attenuated the LPS-mediated induction of IL-12 p40 in BMDCs and bone marrow-derived macrophages (BMDMs) in a dose-dependent manner (Figures 1E and S5), which is consistent with previous reports (Gottfried et al., 2006; Nasi et al., 2013). Furthermore, we confirmed that acidity (pH 6–7) mimicked the effects of lactate on IL-12 p40, and the significant inhibitory effect of lactate on LPS-mediated induction of IL-12 p40 levels in BMDCs was eliminated upon neutralization of lactate using $NaHCO_3$ (Figure 1F). This result suggests that acidity decreased the expression of IL-12

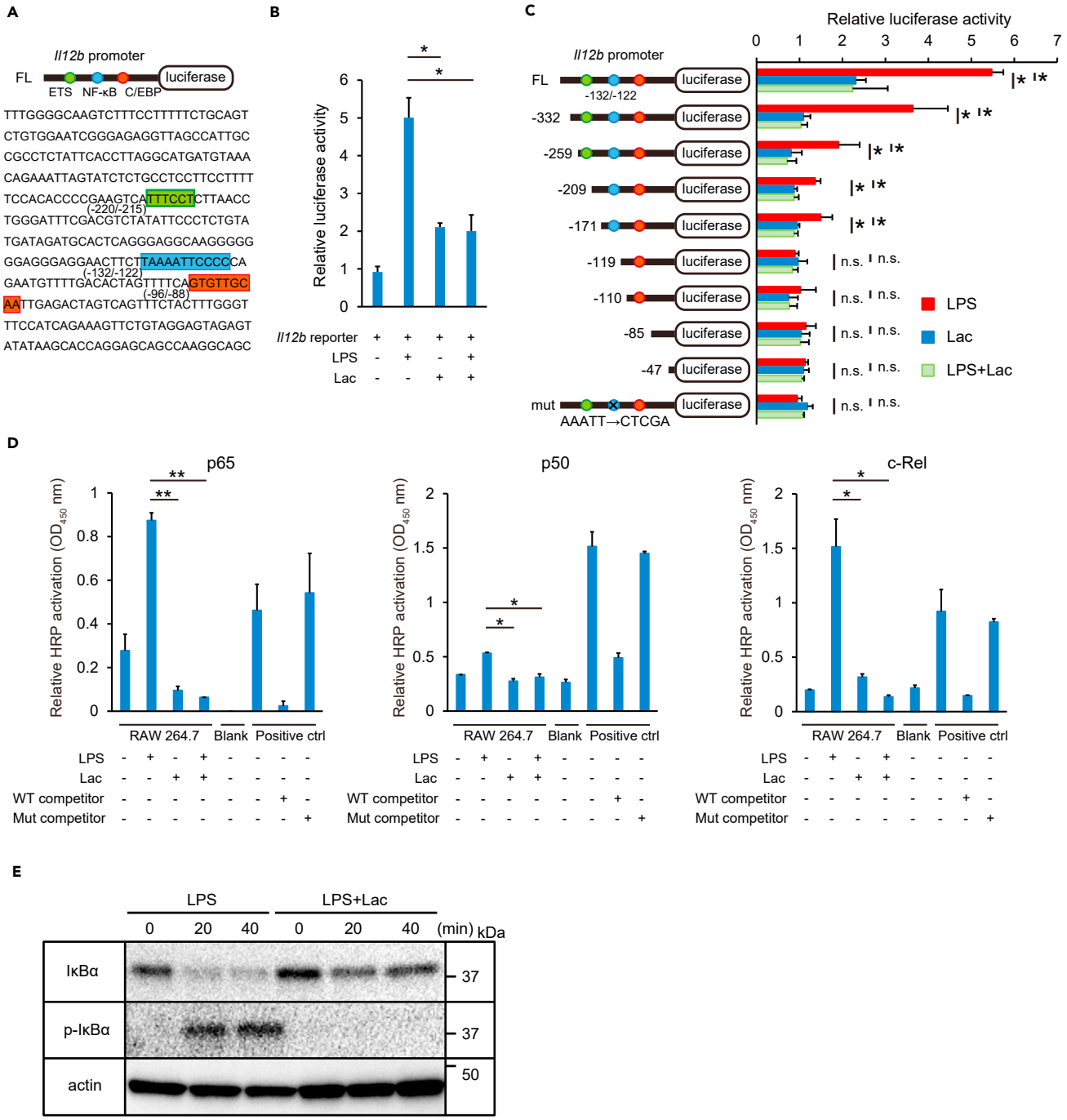

Figure 2. Lactate (Lac) suppresses NF-κB DNA-binding activity to the *Il12b* promoter

(A) A schematic of the luciferase reporter construct with the mouse *Il12b* promoter (top) and the mouse *Il12b* promoter sequence (bottom). Potential binding sites and consensus sequences for the transcription factors ETS (green), NF-κB (blue), and C/EBP (red) are shown.

(B) Luciferase assays. The mouse *Il12b* promoter luciferase reporter construct was transfected into RAW 264.7 cells. Cells were activated with LPS (100 ng/mL) and/or Lac (20 mM) at 24 hr post-transfection, and luciferase activity was measured 24 hr after stimulation. Relative luciferase activity was determined compared with non-activated control cells.

(C) Luciferase assays with deletion mutants and a substitution mutant (mut) of the *Il12b* promoter. Full-length (FL) or mutant constructs were transfected into RAW 264.7 cells. After 24 hr, cells were activated with LPS (100 ng/mL) and/or Lac (20 mM) for 24 hr. Relative luciferase activity was determined compared with non-activated control cells.

(D) The DNA-binding activity of NF-κB p65, p50, and c-Rel was measured with a TransAM NF-κB Transcription Factor Assay Kit.

Figure 2. *Continued*

(E) The IκBα and p-IκBα expressions in cytosolic extracts of RAW 264.7 activated with LPS (100 ng/mL) and/or Lac (20 mM) for 0, 20 or 40 min were analyzed by Western blotting.

Data are expressed as mean ± SD. Significance was analyzed using a two-tailed Student's t-test, Welch's t test, or Mann-Whitney's U test. *$p < 0.05$; **$p < 0.01$; n.s., not significant ($p > 0.05$). See also Figure S7.

p40 in BMDCs. We further examined the actual pH values in human melanoma and mouse tumor tissues. We found that the pH values of both tumor issues were approximately 6–7, and the tumor weights correlated with lactate levels in B16-F1 cell-derived tumors (Figure S6). Taken together, these results suggest that lactate suppressed the LPS-mediated induction of IL-12 p40, likely depending on its acidity.

Lactate suppresses NF-κB DNA-binding activity to the *Il12b* promoter

The inhibition of LPS-mediated induction of IL-12 p40 levels by lactate led us to hypothesize that lactate might affect IL-12 p40 gene levels by regulating transcription factors on the *Il12b* promoter. We first performed luciferase reporter assays using a construct with the *Il12b* promoter upstream of a luciferase reporter gene (Figure 2A). Luciferase activities were suppressed by the addition of lactate to cells treated with LPS compared with only LPS stimulation (Figure 2B). To identify the *Il12b* promoter elements that are important for transcriptional regulation by lactate, we next performed serial deletion and substitution mutant analyses. Deletion of the NF-κB binding site, but not the E26 transformation-specific (ETS) binding site, eliminated the inhibitory effect of lactate on LPS-mediated luciferase reporter activity (Figure 2C). The construct containing only the CCAAT/enhancer-binding protein (C/EBP) binding element did not show significant activation by LPS or lactate. In addition, mutation of the NF-κB binding site in the reporter construct eliminated the inhibition of luciferase reporter activity induced by lactate (Figure 2C). These results indicate that the NF-κB binding sequence in the *Il12b* promoter is important for the transcriptional suppression of *Il12b* by lactate.

We next evaluated the influence of lactate on the DNA-binding activity of NF-κB. Downregulation of the DNA-binding activity of NF-κB p65, p50, and c-Rel subunits was observed in nuclear extracts from cells stimulated with lactate compared with nuclear extracts from LPS-stimulated cells (Figure 2D). Similarly, LPS-induced NF-κB p65 DNA-binding activity was decreased in acidic conditions (pH 6.0), which suggests that the effect of lactate on NF-κB transcriptional activity may depend on acidity (Figure S7). Additionally, silencing of GPR81, a receptor for lactate, attenuated the suppressive effect of lactate on the NF-κB p65 DNA-binding activity, which is consistent with the previous report (Yang et al., 2020). These results suggest that both the acidity of lactate and the signaling pathway through GPR81 may be important in the suppressive effect of lactate on NF-κB p65 DNA-binding activity.

We also considered how lactate suppressed p65 DNA-binding activity. We found that IκBα expression levels were higher in LPS plus lactate-stimulated BMDCs than in LPS-stimulated BMDCs (Figure 2E). In addition, phospho-IκBα expression levels were decreased in LPS and lactate-stimulated BMDCs compared with levels in cells stimulated with LPS only. Taken together, these results suggest that lactate causes suppressed phosphorylation of IκBα, which leads to IκBα accumulation and subsequent inhibition of NF-κB. This eliminates the ability of NF-κB to interact with the NF-κB binding site in the *Il12b* promoter and leads to reduction of IL-12 p40 expression.

Lactate promotes the expression of transcription factor EGR1 in DCs

We performed a comprehensive gene expression analysis, including transcription factor genes, in BMDCs treated with LPS, lactate, and LPS together with lactate. Microarray analyses showed that the early growth response protein 1 (EGR1) transcription factor gene was the most highly expressed gene in BMDCs stimulated by lactate, as well as LPS plus lactate (Figure 3A). Notably, the gene expression of EGR1 was induced by lactate to higher levels compared with other transcription factor genes including the NF-κB family. The induction of EGR1 by lactate was confirmed by Western blotting (Figure 3B). Immunohistochemistry showed that lactate-induced EGR1 localized in the cytoplasm and partially in the nucleus (Figure 3C).

Because EGR1 has been reported to be induced by stress signals by the MAPK signaling pathway (Lim et al., 1998), we speculated that stress signals related to acidity from lactate may lead to EGR1 expression. We confirmed that EGR1 was induced by acidity (pH 6.0), and increased expressions of phospho-p38 and phospho-JNK were observed in lactate-treated BMDCs compared with control BMDCs (Figure S8). We

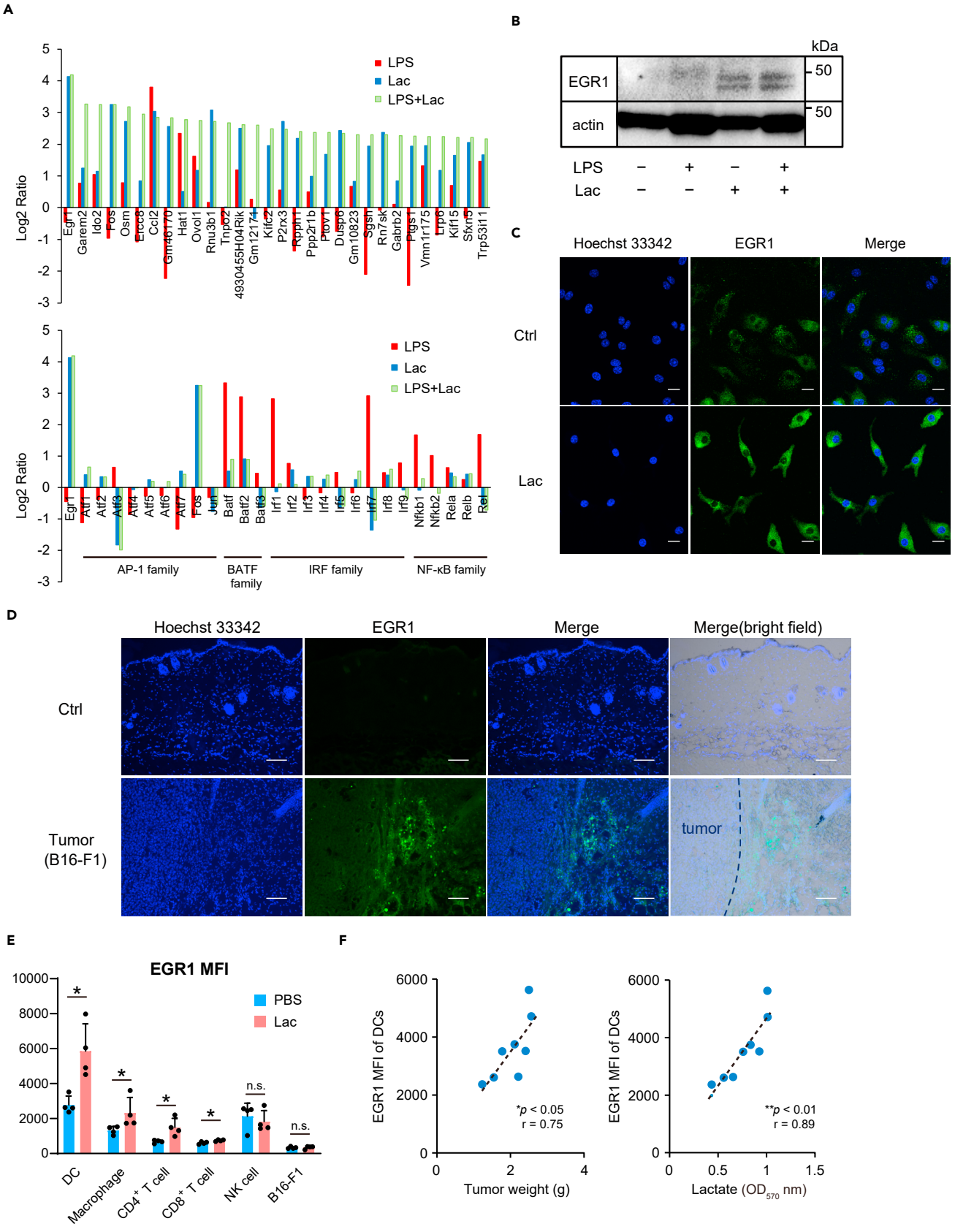
A
LPS
Lac
LPS+Lac
Log2 Ratio
Egr1 Garem2 Ido2 Fos Osm Ercc8 Ccl2 Gm48170 Hat1 Ovol1 Rnu3b1 Tnpo2 4930455H04Rik Gm12174 Kifc2 P2rx3 Rpph1 Ppp2r1b Prov1 Dusp6 Gm10823 Sgsh Rn7sk Gabrb2 Ptgs1 Vmn1r175 Trp6 Klrf15 Sfxn5 Trp53i11
Egr1 Atf1 Atf2 Atf3 Atf4 Atf5 Atf6 Atf7 Fos Jun Batf Batf2 Batf3 Irf1 Irf2 Irf3 Irf4 Irf5 Irf6 Irf7 Irf8 Irf9 Nfkb1 Nfkb2 Rela Relb Rel
AP-1 family
BATF family
IRF family
NF-κB family
B
kDa
EGR1
actin
50
50
LPS − + − +
Lac − − + +
C
Hoechst 33342
EGR1
Merge
Ctrl
Lac
D
Hoechst 33342
EGR1
Merge
Merge(bright field)
Ctrl
Tumor (B16-F1)
tumor
E
EGR1 MFI
PBS
Lac
DC
Macrophage
CD4+ T cell
CD8+ T cell
NK cell
B16-F1
n.s.
F
EGR1 MFI of DCs
Tumor weight (g)
*p < 0.05
r = 0.75
Lactate (OD570 nm)
**p < 0.01
r = 0.89

Figure 3. Lactate (Lac) induces the expression of early growth response protein 1 (EGR1)

(A) BMDCs from WT mice were stimulated with LPS (100 ng/mL) and/or Lac (20 mM) for 4 hr, and the total RNA from these cells was subjected to microarray analysis. The log2 ratios for the indicated genes in BMDCs stimulated with LPS plus Lac are arranged in descending order.

(B) Western blot analysis of EGR1 expression in BMDCs stimulated with LPS (100 ng/mL) and/or Lac (20 mM) for 24 hr.

(C) EGR1 expression (green) in RAW 264.7 cells stimulated with Lac (20 mM) or control medium (Ctrl) for 24 hr. Nuclei were stained with Hoechst 33,342 (blue). Scale bars = 10 μm.

(D) Tumor tissues or control normal skin (Ctrl) from WT mice at two weeks after B16-F1 cell implantation were examined for EGR1 expression (green). Scale bars = 100 μm.

(E) Median fluorescence intensity (MFI) of EGR1 in leukocyte subpopulations in tumor tissues of WT mice 3 weeks post-B16-F1 cell implantation was analyzed using flow cytometry. On days 6, 9 and 12 after injection of B16-F1 cells, Lac (5 mM, 200 μL) or PBS control (200 μL) was intratumorally administered. Data are expressed as mean ± SD.

(F) The relationship between EGR1 MFI of tumor-infiltrating DCs and tumor weight (left) or lactate level (right) in the tumor tissues of WT mice 3–4 weeks post-B16-F1 cell implantation. Individual findings are plotted and each data point represents one mouse.

Significance was analyzed using a two-tailed Student's t-test, Welch's t test, or Mann–Whitney's U test. Pearson's correlation coefficient was used to evaluate the correlations. *$p < 0.05$; **$p < 0.01$; n.s., not significant ($p > 0.05$). See also Figures S8 and S9.

examined other cell types and found that lactate slightly induced the expression of EGR1 in $CD4^+$ T cells and $CD8^+$ T cells but not in NK cells and B16-F1 melanoma cells (Figure S9).

Based on the results of the increased expression of EGR1 induced by lactate, we hypothesized that the expression levels of EGR1 in tumor tissues may be increased by tumor-derived lactate induced by the Warburg effect. We first examined the expression levels of mouse EGR1 in tumors from the mouse model established by subcutaneous injection with B16-F1 melanoma cells. We found that EGR1 was expressed in tumor tissues but not in normal skin (Figure 3D). Flow cytometric analyses revealed that the EGR1 mean fluorescence intensity (MFI) was higher in DCs in B16-F1 cell-derived tumors compared with other immune cells or tumor cells (Figure 3E). Additionally, the EGR1 MFI in DCs, macrophages, $CD4^+$ T cells, and $CD8^+$ T cells was increased in mice treated with lactate compared with those with PBS. The EGR1 MFI of DCs correlated with tumor weight and lactate levels in tumor tissues (Figure 3F).

Next, we investigated the expression of EGR1 in 19 human melanoma tissue samples (Table S1). We found a significant increase in EGR1-positive expression in tumor tissues of patients with invasive melanoma compared with primary tissues of non-invasive melanoma *in situ* (Figures 4A and 4B). Additionally, we found a correlation of the EGR1-positive ratio with tumor thickness as well as serum 5-S-cysteinyl-DOPA level, which is a common tumor marker for melanoma (Figure 4C). $CD11c^+$ DCs highly expressed EGR1, while the expression of EGR1 was moderate in other cell types (Figure 4D). Finally, database analyses using TCGA revealed a correlation between EGR1 expression and the expression of lactate dehydrogenase (LDHA), a glycolytic marker, in primary invasive melanoma (Figure 4E). Collectively, these data show that EGR1 was expressed in DCs and its expression was increased in primary invasive melanoma tissues and correlated with LDHA, suggesting that the expression of EGR1 induced by lactate may have some role in DC function within the tumor microenvironment.

CD80 expression is increased EGR1-deficient DCs

Our data suggest that EGR1 induced by lactate may be important for DC function. Therefore, we performed analyses using BMDCs from *Egr1*$^{-/-}$ mice (Figure S10) compared with DCs from WT mice. To investigate the effect of EGR1 on cytokine expression, we performed ELISAs to examine the levels of IL-12 p40, TNF-α, and IL-6 secreted by *Egr1*$^{-/-}$ and WT BMDCs following stimulation by LPS. However, there were no significant differences in IL-12 p40, TNF-α, and IL-6 levels in culture medium of *Egr1*$^{-/-}$ BMDCs and WT BMDCs (Figure 5A). We also did not detect significant differences in the number of splenic macrophages, DCs, or T cells between *Egr1*$^{-/-}$ and WT controls (Figure S11).

We next performed microarray analysis using *Egr1*$^{-/-}$ and WT BMDCs (Figure 5B). Within the KEGG category of the cell adhesion molecules and TLR signaling pathways, *Cd80*, *Cd86*, and *Cd40* overlapped. Among the three genes, *Cd80* showed the greatest increase in expression in *Egr1*$^{-/-}$ DCs compared with WT DCs, and a significant increase of CD80 expression in *Egr1*$^{-/-}$ DCs was also confirmed using flow cytometric analysis (Figure 5C). Furthermore, lactate reduced LPS-induced CD80 MFI in BMDCs, and the MFI of CD80 was higher in *Egr1*$^{-/-}$ BMDCs compared with WT BMDCs treated with LPS and lactate (Figure 5D). Antigen presentation assays revealed increased proliferation of OT-I $CD8^+$ cells cultured with *Egr1*$^{-/-}$ BMDCs compared with those cultured with WT BMDCs (Figure 5E). However, there were no

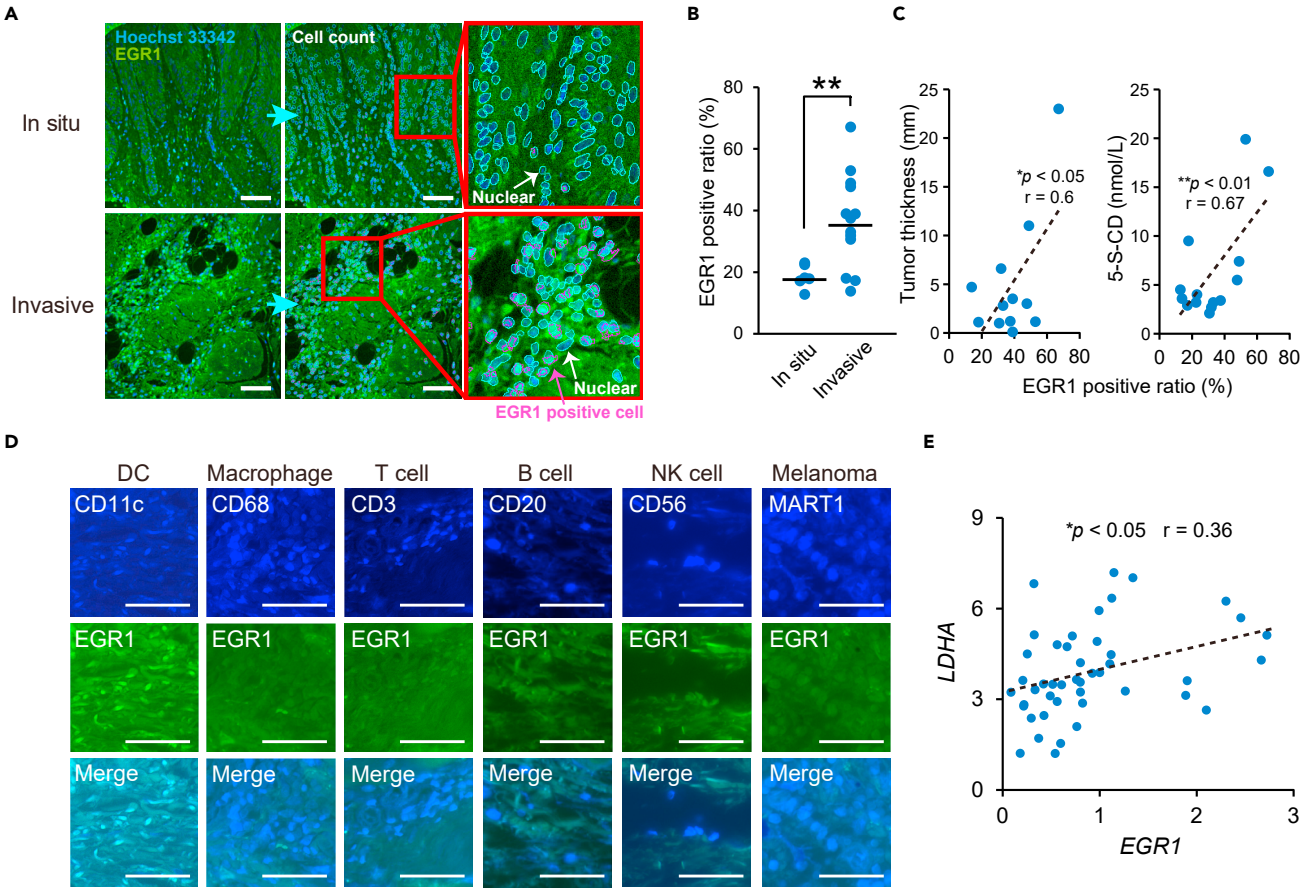

Figure 4. *EGR1* is expressed in DCs and correlates with *LDHA* in human melanoma tissues

(A) Tumor tissues from patients with melanoma *in situ* and invasive melanoma were examined by fluorescent staining (Hoechst 33,342, blue), as well as by immunofluorescence analysis for EGR1 (green). Nuclei (enclosed within light blue lines) and EGR1-positive cells (enclosed within magenta lines) were counted automatically using the In Cell Analyzer software. Scale bars = 50 μm.

(B) EGR1-positive ratios in tumor tissues of melanoma *in situ* and invasive melanoma are plotted (see also Table S1). Each data point represents one patient. Bars indicate the mean.

(C) Relationship between EGR1-positive ratio and tumor thickness (left) or serum 5-S-cysteinyl-DOPA (5-S-CD) levels (right). Individual findings are plotted and each data point represents one patient.

(D) Primary tumor tissues from patients with invasive melanoma were examined by fluorescent staining as indicated. Scale bars = 50 μm.

(E) Correlation analysis of *EGR1* and *LDHA* expression levels using RNA-seq data set acquired from primary tumors from 45 skin cutaneous melanoma patients in TCGA (TCGA-SKCM).

Significance was analyzed using a two-tailed Student's t-test, Welch's t test, or Mann–Whitney's U test. Pearson's correlation coefficient was used to evaluate the correlations. $*p < 0.05$; $**p < 0.01$.

significant differences in tumor growth between *Egr1*$^{-/-}$ and WT mice, and the anti-tumor efficacy of anti-PD-L1 was similar between *Egr1*$^{-/-}$ and WT mice (Figure 5F). Similarly, there were no significant differences in tumor growth between *Egr1*$^{-/-}$ and WT mice treated with 5 mM lactate (Figure 5G).

We speculated these results may be because whole body EGR1-knockout mice were used, and thus other immune cells were affected by EGR1 depletion. Therefore, we performed similar experiments using CD11c-DTR bone marrow chimeric mice and found that tumor growth was suppressed in DC-depleted mice transferred with *Egr1*$^{-/-}$ BMDCs compared those transferred with WT BMDCs (Figure 5H). These results suggest that EGR1-expressing DCs have pro-tumor activities.

Based on the result of increased expression of CD80 in *Egr1*$^{-/-}$ BMDCs, we analyzed the status of H3K27Ac in LPS and lactate-stimulated WT and *Egr1*$^{-/-}$ BMDCs using ChIP-sequencing (ChIP-seq). Contrary to our expectations, the H3K27Ac status on the *Cd80* gene region was comparable between WT and *Egr1*$^{-/-}$

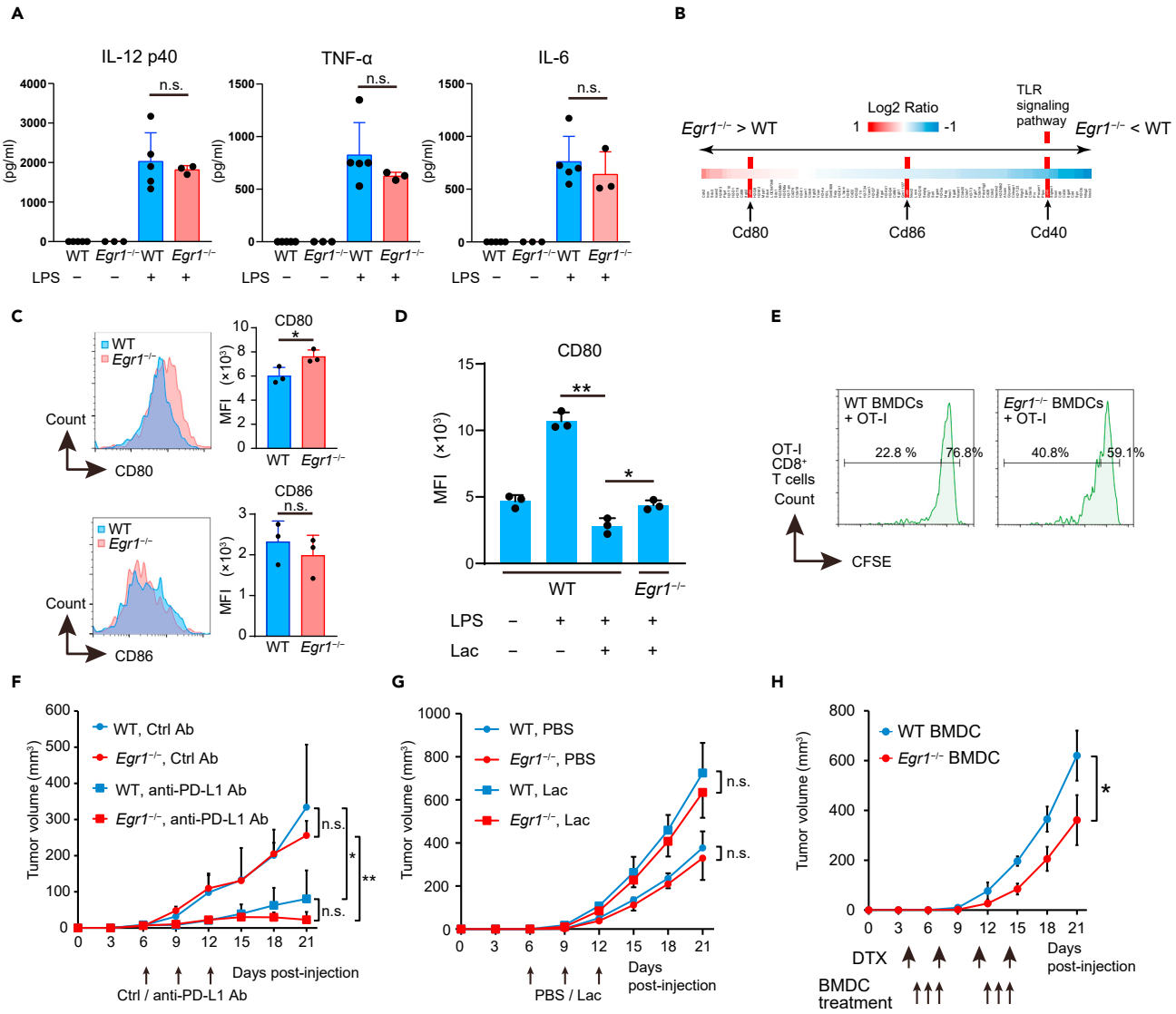

Figure 5. CD80 expression level is increased EGR1-deficient DCs

(A) Levels of IL-12 p40, TNF-α, and IL-6 secreted by BMDCs stimulated with LPS (100 ng/mL) for 24 hr were measured by ELISA. Data are expressed as mean ± SD from two independent experiments (n = 3–5).

(B) RNA from BMDCs from WT and *Egr1*$^{-/-}$ mice was subjected to microarray analysis. The log2 ratio was determined for the corresponding genes categorized in cell adhesion molecules within KEGG pathways and the results were arranged in descending order. Genes that overlapped with TLR signaling pathways are in red boxes.

(C) Flow cytometric analyses of CD80 and CD86 in CD11c^{+} DCs within splenocytes from WT and *Egr1*$^{-/-}$ mice. Representative plots are shown (left). Data are expressed as mean ± SD from two independent experiments (right, n = 3). MFI, median fluorescence intensity.

(D) BMDCs from WT or *Egr1*$^{-/-}$ mice were stimulated with LPS (100 ng/mL) and/or lactate (Lac, 20 mM) for 24 hr and the MFI of CD80 was assessed (n = 3). Data are expressed as mean ± SD.

(E) CFSE-labeled CD8^{+} T cells from OT-I transgenic mice were co-cultured with BMDCs from WT or *Egr1*$^{-/-}$ mice pulsed with Ova 257–264 peptide. Proliferation of OT-I CD8^{+} T cells was assessed after 72 hr by flow cytometry.

(F and G) Tumor growth kinetics in WT or *Egr1*$^{-/-}$ mice subcutaneously injected with 1 × 10^{6} B16-F1 melanoma cells and treated with anti-PD-L1 antibody or control antibody (Ctrl), Lac and/or PBS as indicated. On days 6, 9, and 12 after injection of B16-F1 cells, 200 μg of control IgG Ab or anti-PD-L1 Ab were injected intraperitoneally (F), and Lac (5 mM, 200 μL) or PBS control (200 μL) was intratumorally administered (G). Data are shown as mean ± SD of 3–4 mice per group.

(H) Tumor growth kinetics in diphtheria toxin (DTX)-treated CD11c-DTR bone marrow chimeric mice with subcutaneous injection with 1 × 10^{6} B16-F1 melanoma cells and treated intratumorally with 1×10^{6} WT or *Egr1*$^{-/-}$ BMDCs. Data are shown as mean ± SD (n = 4 mice per group).

Significance was analyzed using a two-tailed Student's t-test, Welch's t test, or Mann–Whitney's U test. *$p < 0.05$; **$p < 0.01$; n.s., not significant ($p > 0.05$).

See also Figures S10 and S11.

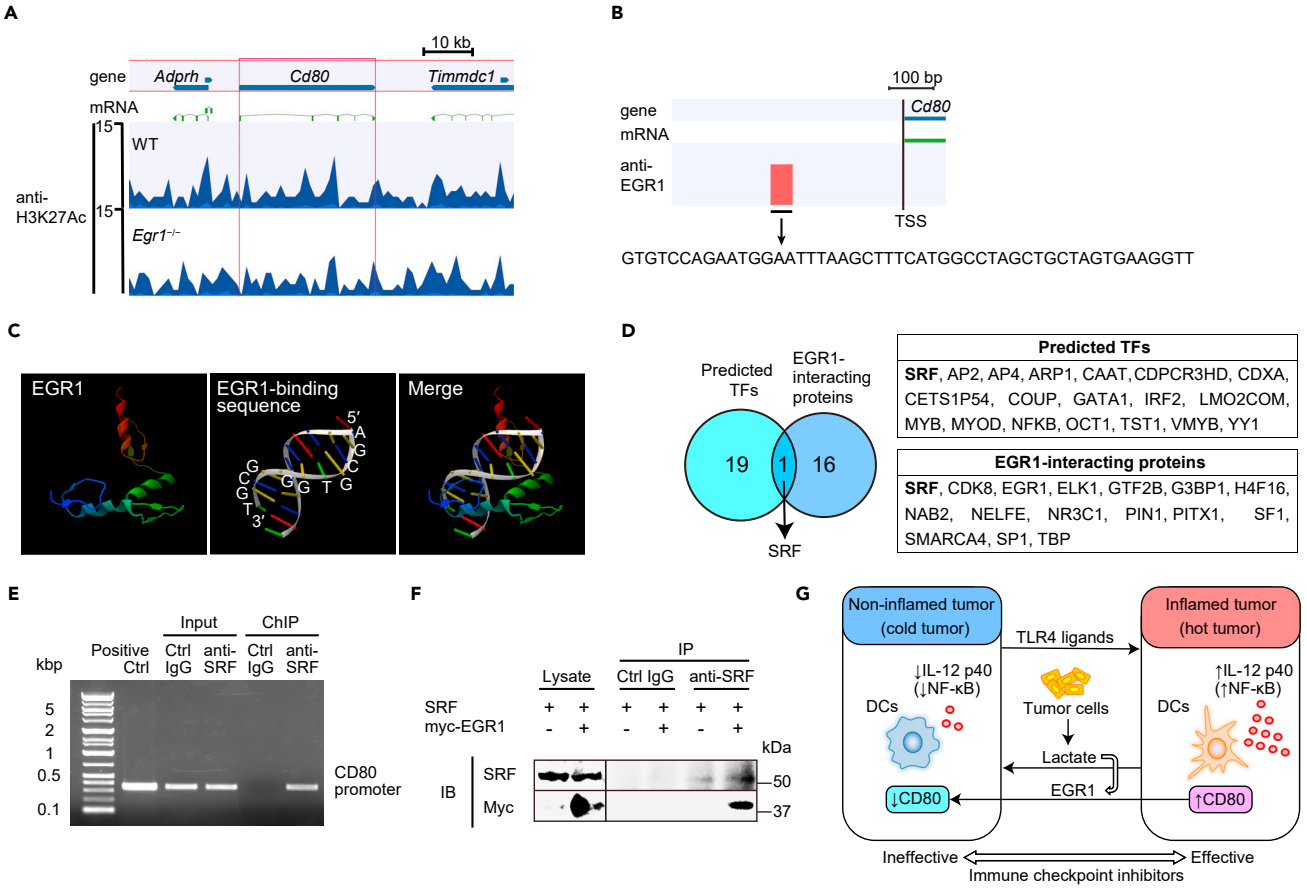

Figure 6. EGR1 interacts with SRF and may regulate its activation on the *Cd80* promoter

(A) ChIP-seq enrichment profiles for H3K27Ac at the *Cd80* locus were generated using WT or *Egr1*$^{-/-}$ BMDCs stimulated with LPS (100 ng/mL) and lactate (Lac, 20 mM) for 24 hr.

(B) ChIP-seq enrichment profiles for EGR1 at the transcription start site (TSS) at the *Cd80* locus were generated using WT BMDCs stimulated by LPS (100 ng/mL) and Lac (20 mM) for 24 hr.

(C) The 3D protein structure of EGR1 and the EGR1 binding sequence from Protein DataBank were analyzed by CLC Genomics Workbench.

(D) SRF was predicted as a potential transcription factor that binds to the region identified in (B) using TFBIND software. SRF was previously reported to interact with EGR1. TF, transcription factor.

(E) ChIP-PCR analysis was performed using RAW 264.7 cells overexpressing *Srf*. ChIP was performed using control IgG (Ctrl) or anti-SRF antibody. PCR was performed using primers that detect sequences in the *Cd80* promoter.

(F) Co-immunoprecipitation experiments assessing EGR1 binding to SRF. Cell extracts from RAW 264.7 cells overexpressing both *Srf* and Myc-tagged *Egr1* were immunoprecipitated with anti-SRF antibody or control IgG (Ctrl) and analyzed with anti-c-Myc and anti-SRF antibody by Western blotting.

(G) Proposed schematic model of how lactate and its induction of EGR1 switches a hot tumor to a cold tumor. Lactate induces a shift from a hot tumor (presence of inflammation) to a cold (non-inflamed) tumor, while TLR4 ligands cause the opposite shift. Lactate upregulates the expression of EGR1, which may downregulate the expression of CD80.

See also Figures S12–S14.

BMDCs (Figure 6A). The H3K27Ac status on *Il12b*, *Il6*, *Tnf*, and *Cd86* gene regions were also similar between WT and *Egr1*$^{-/-}$ BMDCs (Figure S12). Next, we analyzed the proximal TSS region on *Cd80* promoter by ChIP-seq using anti-EGR1 antibody and identified a potential EGR1-interacting region (Figure 6B). We searched for potential transcription factors that bind to the identified region using CLC Genomics Workbench and TFBIND software (Tsunoda and Takagi, 1999). Analysis of the 3D protein structure from Protein DataBank (Elrod-Erickson et al., 1996) and TFBIND analysis did not identify any EGR1-binding sequence in the CD80 promoter (Figure 6C). NF-κB was predicted as a potential transcription factor that binds to this region; however, the NF-κB p65 DNA-binding activities were similar between nuclear extracts overexpressing EGR1 and controls (Figure S13). Serum response factor (SRF) was also predicted as a potential transcription factor that binds to this region, and SRF was previously reported to interact with EGR1 (Wang et al., 2005) (Figure 6D). Another study also reported that *Cd80* was downregulated in *Srf*$^{-/-}$ neutrophils

compared with WT neutrophils in RNA deep sequencing (Taylor et al., 2014). Our ChIP-PCR analysis using SRF antibody also demonstrated that SRF interacted with the CD80 promoter (Figure 6E). Therefore, we hypothesized that EGR1 might interact with the CD80 promoter through binding to SRF. Co-immunoprecipitation experiments revealed that EGR1 interacts with SRF (Figure 6F), which is consistent with the previous report (Wang et al., 2005). Additionally, ChIP-PCR analysis in cells knocked down for SRF by siRNA demonstrated that EGR1 binding on the CD80 promoter was lost when SRF was silenced (Figure S14). Taken together, these results suggest that EGR1 interacts with SRF and may regulate its activation on the *Cd80* promoter.

DISCUSSION

Since the demonstrated clinical success of ICIs, one of the most active research focuses today is augmenting the responses to ICIs by targeting the tumor microenvironment (Chen and Mellman, 2017). Tumors with an inflamed tumor microenvironment are considered "hot tumors" and show good responses to ICIs. Our results show that lactate inhibited the effects of ICI in a mouse tumor model, indicating that lactate is possibly associated with one of the mechanisms of the cooling switch. LPS-induced anti-tumor cytokines and molecules, such as IL-12 p40 and CD80, were decreased by lactate in DCs, which suggests that DCs can be directed to non-inflammatory conditions by lactate. Luciferase assays showed that suppression of the DNA-binding activity of NF-κB by lactate is important for the regulation of IL-12 p40. Our results suggested that lactate causes suppressed phosphorylation of IκBα, which leads to IκBα accumulation and subsequent inhibition of NF-κB. These results were consistent with the recent report showing that lactate attenuated LPS-stimulated macrophage TNF-α and IL-6 production and suppressed LPS-stimulated NF-κB (Yang et al., 2020). Acidity also mimicked the effects of lactate on IL-12 p40, EGR1 and NF-κB activation; therefore, we speculate the effects of lactate on DCs may be from the acidity. Our results also indicate that lactate mediates the suppressive effect on NF-κB activation via GPR81, which was consistent with a previous report (Yang et al., 2020). Together, our findings suggest that both the acidity of lactate and the signaling pathways through GPR81 may be important in the suppressive effect of lactate on NF-κB p65 DNA-binding activity.

Despite the remarkable suppression of NF-κB activity by lactate, microarray analysis showed that the decrease of NF-κB family mRNAs by lactate was mild. Conversely, the EGR1 gene was the most highly induced transcription factor in DCs stimulated with lactate. EGR1 is an inflammatory transcriptional factor (Sukhatme, 1990) that regulates a large set of inflammatory genes, such as IL-2 and TNF-α genes (Krämer et al., 1994; Skerka et al., 1995). Aberrant EGR1 expression is linked to various human diseases including cancers (Bhattacharyya et al., 2013). With database analysis using TCGA, we identified a correlation between *EGR1* and *LDHA* expression in primary melanoma. As LDHA is a glycolytic marker, this result suggests the association of EGR1 with glycolysis. Additionally, histological analysis showed that the expression of EGR1 was increased in human primary invasive melanoma tissues, and $CD11c^+$ DCs expressed EGR1 in human melanoma. Studies have shown that as tumor thickness increases, there is a significant decrease in survival rates (Balch et al., 2009). Therefore, increased EGR1 expression might be a marker of invasive melanoma. Consistent with these observations, the expression levels of EGR1 were correlated with tumor thickness and 5-S-cysteinyl-DOPA, which is correlated with prognosis in melanoma (Bánfalvi et al., 2003). Notably, these results are preliminary findings, as the number of human samples was small; therefore, further studies with a larger sample number are needed.

We hypothesized that EGR1 might be a key transcription factor to regulate cytokines and co-stimulatory factors in DCs. However, there were no significant differences in the expression levels of IL-12 p40, TNF-α, and IL-6 between $Egr1^{-/-}$ and WT BMDCs. However, CD80 was increased in $Egr1^{-/-}$ BMDCs compared with WT BMDCs. These results were consistent with the recent report that *Egr1* silencing led to elevated expression of CD80 in toxoplasma-infected DCs and LPS-challenged immature DCs (Ten Hoeve et al., 2019). Despite the significant difference of the expression of CD80 and antigen presentation assay *in vitro*, the B16-F1 cell–derived tumor growth rate was similar between WT and $Egr1^{-/-}$ mice. Consistent with these findings, Caso et al. reported reduced growth of Lewis lung carcinoma but not B16-F10 cell-derived tumors in $Egr1^{-/-}$ mice. Fahmy et al. also reported similar results, which suggest other EGR1 mechanisms, including FGF-dependent angiogenesis during neovascularization and tumor growth by EGR1 (Fahmy et al., 2003). Therefore, to eliminate the possible effect of EGR1 in other cells except DCs, we used a DC-specific knockout model and found that tumor growth was suppressed in DC-depleted mice transferred with $Egr1^{-/-}$ BMDCs compared those transferred with WT BMDCs. These results suggest that EGR1 in DCs has a pro-tumor activity.

ChIP-Seq results identified a region with a potential interaction site for EGR1 in the *Cd80* promoter. The region was not identical to the EGR1-binding sequence, according to the analysis by TFBIND and data from Protein DataBank. However, our data show that EGR1 interacts with the SRF transcription factor on the *Cd80* promoter. A previous study reported that *Cd80* was downregulated in $Srf^{-/-}$ neutrophils compared with WT neutrophils (Taylor et al., 2014), and thus EGR1 may regulate SRF activation on the *Cd80* promoter. Taken together, these results suggest that the expression of IL-12 p40 can be suppressed by lactate but this is independent of EGR1, while the expression of CD80 may be dependent on both lactate and EGR1, which itself is induced by lactate. Although increased expression of CD80 was observed in $Egr1^{-/-}$ BMDCs compared with WT BMDCs under stimulation of LPS and lactate, the difference was mild. Therefore, our results suggest that lactate suppresses LPS-induced CD80 expression but its suppressive effect via upregulation of EGR1 may be partial.

In conclusion, our results suggest that lactate and its induced EGR1 may be key factors that determine the inflamed or non-inflamed tumor status (Figure 6G). Lactate and EGR1 may be targets for stimulating antitumor immunity and may also be important in cancer treatment with ICIs.

Limitations of the study

Our study has several limitations. Our methods have some artificial aspects as experimental models that may not completely represent real life conditions, such as the possible effect of buffering systems existing *in vivo*. Additionally, lactate has been reported to differentially affect not only DCs but also other tumor infiltrating immune cells, such as $CD8^+$ T cells and Tregs (Haas et al., 2015; Speiser et al., 2016). Therefore, our results may just reflect part of the mechanisms underlying the immunomodulating effect of lactate on immune cells. Therefore, further studies using experimental models that more closely reflect real life tumors are needed to elucidate the full mechanisms of lactate on tumors including other tumor-infiltrating immune cells.

STAR★METHODS

Detailed methods are provided in the online version of this paper and include the following:

- KEY RESOURCES TABLE
- RESOURCE AVAILABILITY
  - Lead contact
  - Materials availability
  - Data and code availability
- EXPERIMENTAL MODEL AND SUBJECT DETAILS
  - Mice
  - Cells
  - Plasmids
  - Tumor model
- METHOD DETAILS
  - *In vivo* anti-PD-L1 antibody and lactate treatment
  - CTL killing assay
  - Antigen-presentation assays
  - Microarray analysis
  - Quantitative PCR
  - ELISA.
  - Immunoblot analysis
  - Flow cytometry
  - Luciferase reporter assays
  - NF-κB DNA-binding assay
  - Histological analysis
  - Analysis of human specimens
  - Tissue digestion for cell population analyses
  - Measurement of lactate concentration in tumors
  - ChIP-seq analysis
  - ChIP-PCR analysis
  - Co-immunoprecipitation

SUPPLEMENTAL INFORMATION

Supplemental information can be found online at https://doi.org/10.1016/j.isci.2021.103067.

ACKNOWLEDGMENTS

This work was supported by the Japan Society for the Promotion of Science (JSPS, Grant Numbers 18H06228, 19K21328 and 20K17353) and Center for Animal Resources and Development of Kumamoto University. We thank Prof. Seiji Okada and Dr. Ryusho Kariya for technical assistance in bone marrow transfer experiments. We thank Gabrielle White Wolf, PhD, from Edanz (https://jp.edanz.com/ac) for editing a draft of this manuscript.

AUTHOR CONTRIBUTIONS

H.Kanemaru, Y.M., S.F. and H.I. developed the concept. H.Kanemaru, A.K. and H.T. designed and performed the experiments and analyzed the data. H.Kanemaru, A.K., T.K., H. Kuriyama, S.S., I.K., K.M., A.M., J.A., T.M., S.M., S.F., and H.I. provided patient specimens and/or clinical data. H.Kanemaru wrote the paper.

DECLARATION OF INTERESTS

The authors declare no potential conflicts of interest.

Received: February 22, 2021
Revised: June 2, 2021
Accepted: August 26, 2021
Published: September 24, 2021

REFERENCES

Bánfalvi, T., Gilde, K., Gergye, M., Boldizsár, M., Kremmer, T., and Ottó, S. (2003). Use of serum 5-S-CD and S-100B protein levels to monitor the clinical course of malignant melanoma. Eur. J. Cancer *39*, 164–169.

Balch, C., Gershenwald, J., Soong, S., Thompson, J., Atkins, M., Byrd, D., Buzaid, A., Cochran, A., Coit, D., Ding, S., et al. (2009). Final version of 2009 AJCC melanoma staging and classification. J. Clin. Oncol. *27*, 6199–6206.

Bhattacharyya, S., Fang, F., Tourtellotte, W., and Varga, J. (2013). Egr-1: new conductor for the tissue repair orchestra directs harmony (regeneration) or cacophony (fibrosis). J. Pathol. *229*, 286–297.

Brand, A., Singer, K., Koehl, G.E., Kolitzus, M., Schoenhammer, G., Thiel, A., Matos, C., Bruss, C., Klobuch, S., Peter, K., et al. (2016). LDHA-associated lactic acid production blunts tumor immunosurveillance by T and NK cells. Cell Metab *24*, 657–671.

Chen, D.S., and Mellman, I. (2017). Elements of cancer immunity and the cancer-immune set point. Nature *541*, 321–330.

Colegio, O.R., Chu, N.Q., Szabo, A.L., Chu, T., Rhebergen, A.M., Jairam, V., Cyrus, N., Brokowski, C.E., Eisenbarth, S.C., Phillips, G.M., et al. (2014). Functional polarization of tumour-associated macrophages by tumour-derived lactic acid. Nature *513*, 559–563.

Delconte, R.B., Kolesnik, T.B., Dagley, L.F., Rautela, J., Shi, W., Putz, E.M., Stannard, K., Zhang, J.G., Teh, C., Firth, M., et al. (2016). CIS is a potent checkpoint in NK cell-mediated tumor immunity. Nat. Immunol. *17*, 816–824.

Dietl, K., Renner, K., Dettmer, K., Timischl, B., Eberhart, K., Dorn, C., Hellerbrand, C., Kastenberger, M., Kunz-Schughart, L.A., Oefner, P.J., et al. (2010). Lactic acid and acidification inhibit TNF secretion and glycolysis of human monocytes. J. Immunol. *184*, 1200–1209.

Dong, H., and Bullock, T.N. (2014). Metabolic influences that regulate dendritic cell function in tumors. Front. Immunol. *5*, 24.

Elrod-Erickson, M., Rould, M.A., Nekludova, L., and Pabo, C.O. (1996). Zif268 protein-DNA complex refined at 1.6 A: a model system for understanding zinc finger-DNA interactions. Structure *4*, 1171–1180.

Fahmy, R.G., Dass, C.R., Sun, L.Q., Chesterman, C.N., and Khachigian, L.M. (2003). Transcription factor Egr-1 supports FGF-dependent angiogenesis during neovascularization and tumor growth. Nat. Med. *9*, 1026–1032.

Fasbender, F., and Watzl, C. (2018). Impedance-based analysis of Natural Killer cell stimulation. Sci. Rep. *8*, 4938.

Fischer, K., Hoffmann, P., Voelkl, S., Meidenbauer, N., Ammer, J., Edinger, M., Gottfried, E., Schwarz, S., Rothe, G., Hoves, S., et al. (2007). Inhibitory effect of tumor cell-derived lactic acid on human T cells. Blood *109*, 3812–3819.

Gottfried, E., Kunz-Schughart, L.A., Ebner, S., Mueller-Klieser, W., Hoves, S., Andreesen, R., Mackensen, A., and Kreutz, M. (2006). Tumor-derived lactic acid modulates dendritic cell activation and antigen expression. Blood *107*, 2013–2021.

Haas, R., Smith, J., Rocher-Ros, V., Nadkarni, S., Montero-Melendez, T., D'Acquisto, F., Bland, E.J., Bombardieri, M., Pitzalis, C., Perretti, M., et al. (2015). Lactate regulates metabolic and pro-inflammatory circuits in control of T cell migration and effector functions. Plos Biol. *13*, e1002202.

Herbst, R.S., Soria, J.C., Kowanetz, M., Fine, G.D., Hamid, O., Gordon, M.S., Sosman, J.A., McDermott, D.F., Powderly, J.D., Gettinger, S.N., et al. (2014). Predictive correlates of response to the anti-PD-L1 antibody MPDL3280A in cancer patients. Nature *515*, 563–567.

Hildner, K., Edelson, B.T., Purtha, W.E., Diamond, M., Matsushita, H., Kohyama, M., Calderon, B.,

Schraml, B.U., Unanue, E.R., Diamond, M.S., et al. (2008). *Batf3* deficiency reveals a critical role for CD8α$^+$ dendritic cells in cytotoxic T cell immunity. Science *322*, 1097–1100.

Hirschhaeuser, F., Sattler, U.G.A., and Mueller-Klieser, W. (2011). Lactate: a metabolic key player in cancer. Cancer Res. *71*, 6921–6925.

Hogquist, K.A., Jameson, S.C., Heath, W.R., Howard, J.L., Bevan, M.J., and Carbone, F.R. (1994). T cell receptor antagonist peptides induce positive selection. Cell *76*, 17–27.

Jung, S., Unutmaz, D., Wong, P., Sano, G., De los Santos, K., Sparwasser, T., Wu, S., Vuthoori, S., Ko, K., Zavala, F., et al. (2002). In vivo depletion of CD11c+ dendritic cells abrogates priming of CD8+ T cells by exogenous cell-associated antigens. Immunity *17*, 211–220.

Kanemaru, H., Yamane, F., Fukushima, K., Matsuki, T., Kawasaki, T., Ebina, I., Kuniyoshi, K., Tanaka, H., Maruyama, K., Maeda, K., et al. (2017). Antitumor effect of *Batf2* through IL-12 p40 up-regulation in tumor-associated macrophages. Proc. Natl. Acad. Sci. U S A. *114*, E7331–E7340.

Kanemaru, H., Yamane, F., Tanaka, H., Maeda, K., Satoh, T., and Akira, S. (2018). BATF2 activates DUSP2 gene expression and up-regulates NF-κB activity via phospho-STAT3 dephosphorylation. Int. Immunol. *30*, 255–265.

Krämer, B., Meichle, A., Hensel, G., Charnay, P., and Krönke, M. (1994). Characterization of an Krox-24/Egr-1-responsive element in the human tumor necrosis factor promoter. Biochim. Biophys. Acta *1219*, 413–421.

Lecoeur, H., Fevrier, M., Garcia, S., Riviere, Y., and Gougeon, M.L. (2001). A novel flow cytometric assay for quantitation and multiparametric characterization of cell-mediated cytotoxicity. J. Immunol. Methods *253*, 177–187.

Lee, S.L., Tourtellotte, L.C., Wesselschmidt, R.L., and Milbrandt, J. (1995). Growth and differentiation proceeds normally in cells deficient in the immediate early gene NGFI-A. J. Biol. Chem. *270*, 9971–9977.

Lim, C.P., Jain, N., and Cao, X. (1998). Stress-induced immediate-early gene, egr-1, involves activation of p38/JNK1. Oncogene *16*, 2915–2926.

Maeda-Otsuka, S., Kajihara, I., Tasaki, Y., Yamada-Kanazawa, S., Sakamoto, R., Sawamura, S., Masuzawa, M., Masuzawa, M., Amoh, Y., Hoshina, D., et al. (2019). Hypoxia accelerates the progression of angiosarcoma through the regulation of angiosarcoma cells and tumor microenvironment. J. Dermatol. Sci. *93*, 123–132.

Murphy, T.L., Cleveland, M.G., Kulesza, P., Magram, J., and Murphy, K.M. (1995). Regulation of interleukin 12 p40 expression through an NF-κB half-site. Mol. Cell. Biol. *15*, 5258–5267.

Nasi, A., Fekete, T., Krishnamurthy, A., Snowden, S., Rajnavölgyi, E., Catrina, A.I., Wheelock, C.E., Vivar, N., and Rethi, B. (2013). Dendritic cell reprogramming by endogenously produced lactic acid. J. Immunol. *191*, 3090–3099.

O'Neill, L.A., Kishton, R.J., and Rathmell, J. (2016). A guide to immunometabolism for immunologists. Nat. Rev. Immunol. *16*, 553–565.

O'Reilly, M.S., Boehm, T., Shing, Y., Fukai, N., Vasios, G., Lane, W.S., Flynn, E., Birkhead, J.R., Olsen, B.R., and Folkman, J. (1997). Endostatin: an endogenous inhibitor of angiogenesis and tumor growth. Cell *88*, 277–285.

Ohashi, T., Aoki, M., Tomita, H., Akazawa, T., Sato, K., Kuze, B., Mizuta, K., Hara, A., Nagaoka, H., Inoue, N., et al. (2017). M2-like macrophage polarization in high lactic acid-producing head and neck cancer. Cancer Sci. *108*, 1128–1134.

Plevy, S.E., Gemberling, J.H., Hsu, S., Dorner, A.J., and Smale, S.T. (1997). Multiple control elements mediate activation of the murine and human interleukin 12 p40 promoters: evidence of functional synergy between C/EBP and Rel proteins. Mol. Cell. Biol. *17*, 4572–4588.

Raychaudhuri, D., Bhattacharya, R., Sinha, B.P., Liu, C.S.C., Ghosh, A.R., Rahaman, O., Bandopadhyay, P., Sarif, J., D'Rozario, R., Paul, S., et al. (2019). Lactate induces pro-tumor reprogramming in intratumoral plasmacytoid dendritic cells. Front. Immunol. *10*, 1878.

Skerka, C., Decker, E.L., and Zipfel, P.F. (1995). A regulatory element in the human interleukin 2 gene promoter is a binding site for the zinc finger proteins Sp1 and EGR-1. J. Biol. Chem. *270*, 22500–22506.

Speiser, D.E., Ho, P.C., and Verdeil, G. (2016). Regulatory circuits of T cell function in cancer. Nat. Rev. Immunol. *16*, 599–611.

Sukhatme, V.P. (1990). Early transcriptional events in cell growth: the Egr family. J. Am. Soc. Nephrol. *1*, 859–866.

Tagawa, H., Kanemaru, H., Kimura, T., Kuriyama, H., Sawamura, S., Kajihara, I., Miyashita, A., Aoi, J., Fukushima, S., and Ihn, H. (2020). BATF2 expression as a novel marker for invasive phenotype in malignant melanoma. J. Dermatol. *47*, e372–e373.

Taylor, A., Tang, W., Bruscia, E.M., Zhang, P.X., Lin, A., Gaines, P., Wu, D., and Halene, S. (2014). SRF is required for neutrophil migration in response to inflammation. Blood *123*, 3027–3036.

Ten Hoeve, A.L., Hakimi, M.A., and Barragan, A. (2019). Sustained Egr-1 response via p38 MAP kinase signaling modulates early immune responses of dendritic cells parasitized by Toxoplasma gondii. Front. Cell. Infect. Microbiol. *9*, 349.

Thevenot, P.T., Sierra, R.A., Raber, P.L., Al-Khami, A.A., Trillo-Tinoco, J., Zarreii, P., Ochoa, A.C., Cui, Y., Del Valle, L., and Rodriguez, P.C. (2014). The stress-response sensor chop regulates the function and accumulation of myeloid-derived suppressor cells in tumors. Immunity *41*, 389–401.

Tsuchiya, N., Zhang, R., Iwama, T., Ueda, N., Liu, T., Tatsumi, M., Sasaki, Y., Shimoda, R., Osako, Y., Sawada, Y., et al. (2019). Type I interferon delivery by iPSC-derived myeloid cells elicits antitumor immunity via XCR1$^+$ dendritic cells. Cell Rep *29*, 162–175.e9.

Tsukamoto, H., Fujieda, K., Miyashita, A., Fukushima, S., Ikeda, T., Kubo, Y., Senju, S., Ihn, H., Nishimura, Y., and Oshiumi, H. (2018). Combined blockade of IL6 and PD-1/PD-L1 signaling abrogates mutual regulation of their immunosuppressive effects in the tumor microenvironment. Cancer Res. *78*, 5011–5022.

Tsunoda, T., and Takagi, T. (1999). Estimating transcription factor bindability on DNA. Bioinformatics *15*, 622–630.

Walenta, S., Wetterling, M., Lehrke, M., Schwickert, G., Sundfør, K., Rofstad, E.K., and Mueller-Klieser, W. (2000). High lactate levels predict likelihood of metastases, tumor recurrence, and restricted patient survival in human cervical cancers. Cancer Res. *60*, 916–921.

Wang, G., Balamotis, M.A., Stevens, J.L., Yamaguchi, Y., Handa, H., and Berk, A.J. (2005). Mediator requirement for both recruitment and postrecruitment steps in transcription initiation. Mol. Cell *17*, 683–694.

Yang, K., Xu, J., Fan, M., Tu, F., Wang, X., Ha, T., Williams, D.L., and Li, C. (2020). Lactate suppresses macrophage Pro-inflammatory response to LPS stimulation by inhibition of YAP and NF-κB activation via GPR81-mediated signaling. Front. Immunol. *11*, 587913.

Zaritskaya, L., Shurin, M.R., Sayers, T.J., and Malyguine, A.M. (2010). New flow cytometric assays for monitoring cell-mediated cytotoxicity. Expert Rev. Vaccin. *9*, 601–616.

STAR★METHODS

KEY RESOURCES TABLE

REAGENT or RESOURCE	SOURCE	IDENTIFIER
Antibodies		
anti-mouse EGR1	Abcam	ab133695
anti-mouse EGR1	Abcam	ab174509
anti-human EGR1	Abcam	ab194357
anti-mouse PD-L1	Abcam	ab213480
anti-c-Myc antibody (Y69)	Abcam	ab32072
anti-β-actin (C4)	Santa Cruz Biotechnology	sc-47778
goat anti-rabbit IgG (H+L)-HRP conjugate	Bio-Rad	170-6515
anti-β-actin-HRP (AC-15)	Abcam	ab49900
FITC anti-mouse CD3	BioLegend	17A2
PE anti-mouse CD80	BioLegend	16-10A1
PE anti-mouse CD86	BioLegend	GL-1
PerCP/Cy5.5 anti-mouse CD11b	BioLegend	M1/70
PerCP/Cy5.5 anti-mouse CD45RA	BD Pharmingen	14.8
PerCP/Cy5.5 anti-mouse CD4	BioLegend	GK1.5
APC anti-mouse F4/80	BioLegend	BM8
APC anti-mouse CD11c	BioLegend	N418
APC anti-mouse CD8a	BioLegend	53-6.7
InVivoMAb anti-mouse PD-L1 (B7-H1)	Bio X Cell	10F.9G2
InVivoMAb rat IgG2b isotype control, anti-keyhole limpet hemocyanin	Bio X Cell	LTF-2
Alexa Fluor 647-goat anti-rabbit IgG (H+L)	Thermo Fisher Scientific	A-21245
anti-EGR1 (used for ChIP)	Cell Signaling Technology	15F7
anti-histone H3 (acetyl K27)	Abcam	ab4729
normal rat IgG	Santa Cruz Biotechnology	sc-2026
rat anti-mouse SRF antibody	Active Motif	2C5
rabbit anti-mouse SRF antibody	Abcam	ab53147
goat anti-rabbit IgG H&L (Alexa Fluor 405)	Abcam	ab175652
APC anti-human CD20 Antibody	BioLegend	2H7
Alexa Fluor 594 anti-human MART-1 antibody	BioLegend	M2-7C10
APC anti-human CD56 (NCAM) antibody	BioLegend	MEM-188
APC anti-human CD68 antibody	BioLegend	Y1/82A
APC anti-human CD11c antibody	BioLegend	3.9
anti-p-p38 antibody (Thr 180/Tyr 182)	Santa Cruz Biotechnology	sc-17852-R
anti-phospho-SAPK/JNK (Thr183/Tyr185)	Cell Signaling Technology	81E11
anti-IκBα mouse antibody	Cell Signaling Technology	L35A5
anti-phospho-IκBα (Ser32/36)	Cell Signaling Technology	5A5
anti-melanoma gp100 antibody	Abcam	ab137078
donkey anti-goat IgG H&L (HRP)	Abcam	ab97110
human/mouse c-Rel antibody	R&D	AF2699
PE anti-EGR1 rabbit antibody	Cell Signaling Technology	44D5
anti-GPR81 antibody	Thermo Fisher Scientific	PA5-67873
Rabbit IgG Isotype Control	Cell Signaling Technology	DA1E

(*Continued on next page*)

Continued

REAGENT or RESOURCE	SOURCE	IDENTIFIER
Chemicals, peptides, and recombinant proteins		
mouse GM-CSF	Prospec	CYT-222
mouse M-CSF	PeproTech	315-02
LPS (LPS-SM ultrapure)	InvivoGen	tlrl-smlps
L-(+)-Lactic acid	Sigma-Aldrich	L6402
Ova 257–264 peptide (SIINFEKL)	MBL	OF1060-B
recombinant mouse IFN-γ (carrier-free)	BioLegend	575306
Hoechst 33342 solution	Dojindo	H342
protein G-Sepharose	Abcam	ab193259
sodium L-lactate	Sigma-Aldrich	71718
diphtheria toxin	Sigma-Aldrich	D0564
collagenase type II	Sigma-Aldrich	C6885
Critical commercial assays		
High Pure RNA Isolation Kit	Roche	11828665001
ReverTra Ace	Toyobo	TRT-101
Real-time PCR Master Mix	Toyobo	QPK-101
mouse IL-12 p40 DuoSet ELISA	R&D	DY-499-05
mouse TNF-α DuoSet ELISA	R&D	DY410-05
mouse IL-6 DuoSet ELISA	R&D	DY406-05
mouse $CD4^+$ T Cell Isolation Kit	Miltenyi Biotec	130-104-454
mouse $CD8^+$ T Cell Isolation Kit	Miltenyi Biotec	130-104-075
mouse NK Cell Isolation Kit II	Miltenyi Biotec	130-096-892
CFSE Cell Division Tracker Kit	BioLegend	423801
Dual-Luciferase Reporter Assay System	Promega	E1910
PrimeSTAR Mutagenesis Basal Kit	Takara	R046A
TransAM NF-κB p65 ELISA kit	Active Motif	40096
TransAM Flexi NF-κB p50	Active Motif	41098
TransAM Flexi NF-κB Family	Active Motif	43298
ChIP-IT Express Enzymatic	Active Motif	53009
Chromatin IP DNA Purification Kit	Active Motif	58002
Foxp3/Transcription Factor Staining Buffer Set	Thermo Fisher Scientific	00-5523-00
FITC Annexin V Apoptosis Detection Kit I	BD Pharmingen	556547
Lactate Assay Kit (Colorimetric)	Cell Biolabs	MET-5012
Deposited data		
BMDC microarray data	This paper	GEO: GSE163978
ChIP-seq data	This paper	GEO: GSE164027
Experimental models: Cell lines		
B16-F1 cells	Riken BRC	RCB2649
RAW 264.7 cells	Riken BRC	RCB0535
Experimental models: Organisms/strains		
Mouse: C57BL/6J	Charles River Laboratories Japan	https://www.crj.co.jp/product/rm/detail/b6j
Mouse: *Egr1*$^{-/-}$	Jackson laboratory	JAX stock #012924, Lee et al., 1995
Mouse: C57BL/6-Tg(TcraTcrb)1100Mjb/J (OT-I)	Jackson laboratory	JAX stock #003831, Hogquist et al., 1994
Mouse: CD11c-DTR	Jackson laboratory	JAX stock #004509, Jung et al., 2002

(*Continued on next page*)

Continued

REAGENT or RESOURCE	SOURCE	IDENTIFIER
Oligonucleotides		
TaqMan probes: 18S rRNA	Thermo Fisher Scientific	Mm03928990_g1
TaqMan probes: *Cd274*	Thermo Fisher Scientific	Mm00452054_m1
TaqMan probes: *Egr1*	Thermo Fisher Scientific	Mm00656724_m1
Genotyping primers for *Egr1*$^{-/-}$ mice, Common: 5′-GGGCACAGGGGATGGGA ATG-3′	Jackson Laboratory	Lee et al., 1995
Genotyping primers for *Egr1*$^{-/-}$ mice, WT: 5′-AACCGGCCCAGCAAGACACC-3′	Jackson Laboratory	Lee et al., 1995
Genotyping primers for *Egr1*$^{-/-}$ mice, Mut: 5′-CTCGTGCTTTACGGTATCGC-3′	Jackson Laboratory	Lee et al., 1995
Primers used for CD80 promoter ChIP analysis Fwd, 5′-TGGCAGTCACTCTGTGTCCAG-3′	This paper	N/A
Primers used for CD80 promoter ChIP analysis Rvs, 5′-CTAGTAAGAGTCTATTGAGG-3′	This paper	N/A
GPR81 siRNAs	Thermo Fisher Scientific	s211558
SRF siRNAs	Thermo Fisher Scientific	s74390
Silencer negative control No. 1 siRNA	Thermo Fisher Scientific	AM4611
Recombinant DNA		
Plasmid: *Egr1*	OriGene Technologies	MC217560
Plasmid: Myc-tagged *Egr1*	OriGene Technologies	MR227136
Plasmid: *Srf*	OriGene Technologies	MC217127
Plasmid: *Il12b* 400bp pro-Luc	Addgene	#20020
Software and algorithms		
FlowJo analysis software V10	Ashland	https://www.flowjo.com/
Developer Toolbox of IN Cell Analyzer	GE Healthcare	https://www.cytivalifesciences.co.jp/catalog/1705.html
CLC Genomics Workbench 10	Qiagen	https://digitalinsights.qiagen.com/products-overview/discovery-insights-portfolio/analysis-and-visualization/qiagen-clc-genomics-workbench/
TFBIND software	RIKEN	Tsunoda and Takagi, 1999
GraphPad Prism v8	GraphPad	https://www.graphpad.com/
Other		
QuantStudio 12K Flex	Applied Biosystems	N/A
Multiskan FC	Thermo Fisher Scientific	N/A
ChemiDoc XRS+ System	Bio-Rad	N/A
NovoCyte	ACEA Biosciences	N/A
xCELLigence S16 system	Agilent Technologies	N/A
Neon Transfection System	Thermo Fisher Scientific	N/A
EnSpire	PerkinElmer	N/A
LB 941	Berthold Technologies	N/A
ABI 3130xl	Applied Biosystems	N/A
BZ-9000	Keyence	N/A
FV1200	Olympus	N/A
IN Cell Analyzer 2200	GE Healthcare	N/A

RESOURCE AVAILABILITY

Lead contact

Further information and requests for resources and reagents should be directed to and will be fulfilled by the Lead Contact, Hisashi Kanemaru (hisashikanemaru@gmail.com).

Materials availability

This study did not generate new unique reagents.

Data and code availability

The microarray and ChIP-seq datasets have been deposited in the NCBI Gene Expression Omnibus (GEO) database (accession no. GSE163978 and GSE164027). This paper does not report original code. Any additional information required to reanalyze the data reported in this paper is available from the lead contact upon request.

EXPERIMENTAL MODEL AND SUBJECT DETAILS

Mice

Mice were maintained in our specific pathogen-free animal facility according to the institutional guidelines. C57BL/6J mice were obtained from Charles River Laboratories Japan. OT-I transgenic mice, *Egr1*$^{-/-}$ mice and CD11c-DTR transgenic mice were obtained from the Jackson Laboratory (Hogquist et al., 1994; Jung et al., 2002; Lee et al., 1995). Experiments were generally performed with female and male mice at 6–12 weeks of age. All animal experiments were performed with approval from the Animal Research Committee of Kumamoto University (Kumamoto, Japan).

Cells

B16-F1 (Riken BRC, Ibaraki, Japan) cells were grown in D-MEM (High Glucose, 043-30085, FUJIFILM Wako, Osaka, Japan) containing 10% fetal bovine serum (FBS). RAW 264.7 (Riken BRC) cells were grown in MEM (Minimum Essential Medium Eagle, M4655, Sigma-Aldrich, St. Louis, MO, USA) containing 10% FBS. BMDCs were generated as described previously (Kanemaru et al., 2017). Briefly, mouse bone marrow cells were obtained from femurs and differentiated into DCs in MEM with 10% FBS containing 10 ng/ml granulocyte macrophage colony-stimulating factor (GM-CSF; Prospec, East Brunswick, NJ, USA). Medium was replaced with fresh medium containing GM-CSF every two days. On day 6, cells were collected. BMDMs were also generated as described previously (Kanemaru et al., 2017). Bone marrow cells were obtained and incubated in MEM with 10% FBS containing 3 ng/ml macrophage colony-stimulating factor (M-CSF, PeproTech, Rocky Hill, NJ, USA). Medium was changed on day 3. On day 5, macrophages were harvested. BMDCs and BMDMs were stimulated with LPS (100 ng/ml; LPS-SM ultrapure, InvivoGen, San Diego, CA, USA) and/or L-(+)-Lactic acid (Sigma-Aldrich), and/or sodium L-lactate (Sigma-Aldrich).

Plasmids

Plasmids encoding *Egr1*, Myc-tagged *Egr1*, and *Srf* were purchased from OriGene Technologies (MC217560, MR227136, and MC217127). Il12b 400bp pro-Luc plasmid was a gift from Dr. Stephen Smale (Addgene plasmid #20020; http://n2t.net/addgene:20020; RRID:Addgene_20020) (Plevy et al., 1997).

Tumor model

B16-F1 cells were grown in DMEM culture media with 10% FBS. Cells were washed with PBS, dispersed in a 0.25% solution of trypsin, and resuspended in fresh culture media. After centrifugation, the cell pellet was resuspended in PBS and the concentration was adjusted to 10^7 cells/ml. Mice were then injected with 0.1 ml of the suspension (1×10^6 B16-F1 cells). Tumors were measured with a dial-caliper every 3 days, and tumor volumes were determined using the formula $(\text{width})^2 \times \text{length} \times 0.52$, as previously described (Colegio et al., 2014; O'Reilly et al., 1997). When the mean tumor diameter reached 1.2 cm, the experiments were terminated, and mice were sacrificed and autopsied.

METHOD DETAILS

In vivo anti-PD-L1 antibody and lactate treatment

In vivo treatment of the tumor mouse model with anti-PD-L1 antibody was performed as previously described (Tsukamoto et al., 2018). On days 6, 9 and 12 after injection of B16-F1 cells, 200 μg of control

IgG Ab (LTF-2, Bio X Cell, Lebanon, NH, USA) or anti-PD-L1 Ab (10F.9G2, Bio X Cell) were injected intraperitoneally. In addition, lactate (5 mM, 200 μl) or PBS control (200 μl) was subcutaneously transferred into the backs of mice on days 6, 9 and 12. The tumors were measured with a dial caliper every 3 days, and the tumor volumes were determined as described above.

Bone marrow transfer experiments were performed as previously described (Kanemaru et al., 2017). Recipient C57BL/6J mice (6 weeks old) were lethally irradiated with 9 Gy and intravenously injected with 2×10^7 bone marrow cells obtained from CD11c-DTR (Itgax-DTR$^{+/-}$) mice. For the depletion of CD11c$^+$ cells, CD11c-DTR bone marrow chimeric mice were intraperitoneally treated with 0.5 μg diphtheria toxin (Sigma-Aldrich) twice per week for a total of four treatments, and mice were treated intratumorally with 1×10^6 BMDCs on days 5, 6, 7, 12, 13, and 14, as previously described (Tsuchiya et al., 2019).

CTL killing assay

The CTL killing assays were performed using the xCELLigence S16 system (Agilent Technologies, Santa Clara, CA, USA) as previously described (Delconte et al., 2016; Fasbender and Watzl, 2018; Hildner et al., 2008; Lecoeur et al., 2001; Zaritskaya et al., 2010). Whole splenocytes (4×10^7) obtained from B16-F1 cell–tumor-bearing WT mice 14 days after implantation were cultured with 2×10^6 IFN-γ-treated (100 U/ml, BioLegend, San Diego, CA, USA) B16-F1 cells. After 5 days, the cells were harvested and used as effector cells in a cytotoxicity assay. As lactate-treated CTLs, effector cells were stimulated with lactate (20 mM) for 24 h. To generate target cells, B16-F1 tumor cells were treated with 100 U/ml IFN-γ for 48 h before use. Target cells were washed and seeded at 20,000 per well into the wells of E-Plates in 150 μl of media. Cell growth was dynamically monitored with the impedance-based xCELLigence S16 system until cells reached log growth phase and formed a monolayer (approximately 18 h). Effector cells were then added directly to individual wells containing the target cells at different ratios (E:T=12.5:1, 25:1, 50:1). For background controls, effector cells were added to wells that contained no target cells, and target cells were added to wells without the addition of effector cells. After addition of effector cells, the system continued to take measurements every 15 min.

Antigen-presentation assays

Antigen-presentation assays were performed as previously described (Hildner et al., 2008; Thevenot et al., 2014). Ovalbumin-specific CD8$^+$ OT-I cells were obtained from mouse spleens and lymph nodes using a CD8$^+$ T Cell Isolation Kit (Miltenyi Biotec, Bergisch Gladbach, Germany). For OT-I T cell proliferation, CD8$^+$ T cells from the splenocytes and lymph nodes of OT-I transgenic mice were labeled with carboxyfluorescein succinimidyl ester (CFSE). BMDCs were pulsed with 1 μM Ova 257-264 peptide (SIINFEKL, MBL, Nagano, Japan) for 3 h, and then cells were washed twice with PBS and co-cultured with 5×10^4 CFSE-labeled naïve OT-I transgenic CD8$^+$ T cells at decreasing dilutions (1:1–1:1/16, OT-I:BMDCs). Proliferation of OT-I cells was measured after 84 h by flow cytometry.

Microarray analysis

BMDCs from WT and *Egr1*$^{-/-}$ mice were stimulated with LPS (100 ng/mL) and/or lactate (20 mM) for 4 h. Total RNA was then isolated using a High Pure RNA Isolation Kit (Roche, Basel, Switzerland) and subjected to Agilent Expression microarray analysis. The microarray was performed by Takara Bio, and the resulting data were analyzed by Aqua (Takara, Shiga, Japan).

Quantitative PCR

RNA was extracted from cells using a High Pure RNA Isolation kit (Roche) according to the manufacturer's instructions. Reverse transcription was performed with 4 μl of ReverTra Ace (Toyobo, Osaka, Japan) in a total volume of 20 μl. Subsequently, 1 μl of cDNA fragments was amplified using 10 μl of real-time PCR Master Mix (Toyobo) with 1 μl of TaqMan probes (Thermo Fisher Scientific, Waltham, MA, USA) in a total volume of 20 μl. Fluorescence from the TaqMan probe for each gene was detected using a QuantStudio 12K Flex (Applied Biosystems, Foster City, CA, USA). The mRNA expression level of each gene was normalized to the 18S rRNA expression level (Mm03928990_g1, Thermo Fisher Scientific). The following TaqMan probes (Thermo Fisher Scientific) were used for quantitative PCR: *Cd274* (Mm00452054_m1) and *Egr1* (Mm00656724_m1).

ELISA.

IL-12 p40, TNF-α, and IL-6 levels were determined by ELISAs (DuoSet ELISA, R&D, Minneapolis, MN, USA) performed according to the manufacturer's instructions. The absorbance of each ELISA plate was measured using a microplate reader (Multiskan FC, Thermo Fisher Scientific).

Immunoblot analysis

Cells were lyzed with lysis buffer (20 mM Tris-HCl [pH 7.5], 150 mM NaCl, 1 mM EDTA, 1% NP40) containing Complete Protease Inhibitor Cocktail (Roche). The cell lysates were separated by standard SDS-PAGE (e-PAGEL, ATTO, Tokyo, Japan) and analyzed by immunoblotting. The following antibodies were used for immunoblotting: anti-PD-L1 (ab213480, Abcam, Cambridge, UK), anti-EGR1 (ab133695, Abcam), anti-c-Myc antibody (Y69) (ab32072, Abcam), goat anti-rabbit IgG (H+L)-HRP Conjugate (Bio-Rad), anti-phospho-p38 antibody (Thr 180/Tyr 182; sc-17852-R, Santa Cruz Biotechnology, Santa Cruz, CA, USA), anti-phospho-SAPK/JNK (Thr183/Tyr185; 81E11, Cell Signaling Technology, Danvers, MA, USA), anti-IκBα mouse antibody (L35A5, Cell Signaling Technology), anti-phospho-IκBα (Ser32/36; 5A5, Cell Signaling Technology), anti-β-actin (C4) (sc-47778, Santa Cruz Biotechnology), and anti-β-actin-HRP (AC-15) (ab49900, Abcam). The Western HRP Substrate (Pierce ECL Western Blotting Substrate, Thermo Fisher Scientific) was used for the development of positive signals, and chemiluminescence was detected using a ChemiDoc XRS+ System (Bio-Rad, Hercules, CA, USA).

Flow cytometry

Cells were washed with magnetic-activated cell sorting buffer, incubated with antibodies for 15 min, and then washed twice. The antibodies for flow cytometry were purchased from commercial sources as follows: anti-CD3-FITC (17A2; BioLegend), anti-CD80-PE (16-10A1; BioLegend), anti-CD86-PE (GL-1; BioLegend), anti-CD11b-PerCP/Cy5.5 (M1/70; BioLegend), anti-CD45RA-PerCP/Cy5.5 (14.8; BD Pharmingen, San Diego, CA, USA), anti-CD4-PerCP/Cy5.5 (GK1.5; BioLegend), anti-F4/80-APC (BM8; BioLegend), anti-CD11c-APC (N418; BioLegend), anti-CD8a-APC (53-6.7; BioLegend), and PE anti-EGR1 rabbit antibody (Cell Signaling Technology). The dilution ratio was 1:100–200 for each antibody. For EGR1 staining, a Foxp3/Transcription Factor Staining Buffer Set (eBioscience, San Diego, CA, USA) was used. Data were collected using a NovoCyte (ACEA Biosciences, San Diego, CA, USA) and analyzed using FlowJo analysis software (Ashland, OR, USA).

Luciferase reporter assays

Luciferase reporter assays were performed according to the manufacturer's instructions (Dual-Luciferase Reporter Assay System, Promega, Madison, WI, USA). For transfections, 1×10^6 RAW 264.7 cells were suspended in 100 μl of a solution (buffer R) containing 8 μg of *Il12b* 400-bp pro-Luc plasmid, and 1 μg of pRL-TK. Cells were electroporated using the Neon Transfection System (Thermo Fisher Scientific) at 1680 V for 20 msec and then plated in a 24-well plate at 1×10^5 cells/well. After 24 h, cells were activated by LPS (100 ng/ml) or lactate (20 mM) for 24 h. Following activation, cell extracts were prepared using Passive Lysis Buffer (Promega). Luciferase activity was determined from a 20-μl cell extract and measured on the EnSpire (PerkinElmer, Waltham, MA, USA) or LB 941 (Berthold Technologies, Bad Wildbad, Germany) microplate reader.

To generate deletion mutants for luciferase reporter assays, mutant DNA fragments were produced by PCR and cloned into the KpnI-BglII sites of the *Il12b* pro-Luc construct as previously described (Murphy et al., 1995). To generate substitution mutants, the mutant constructs were produced using a PrimeSTAR Mutagenesis Basal Kit (Takara) according to the manufacturer's recommendations. All plasmids were verified by restriction mapping and by sequencing using ABI 3130xl (Applied Biosystems).

NF-κB DNA-binding assay

The NF-κB p65 DNA-binding activity was measured with the TransAM NF-κB p65, TransAM Flexi NF-κB p50, and TransAM Flexi NF-κB Family ELISA kit and according to the manufacturer's recommendations (Active Motif, Carlsbad, CA, USA). Nuclear extracts were prepared from 5×10^6 RAW 264.7 cells. After the cells were activated with LPS (100 ng/mL) or lactate (20 mM) for 1 h, cell lysates were prepared in 200 μl lysis buffer [10 mM Hepes-KOH, pH 7.8, 10 mM KCl, 0.1 mM EDTA, pH 8.0, protease inhibitor mixture (Roche), and 0.1% Nonidet P-40], and nuclear extracts were obtained in 60 μl buffer [50 mM Hepes-KOH, pH 7.8, 420 mM KCl, 0.1 mM EDTA, pH 8.0, 5 mM $MgCl_2$, protease inhibitor mixture (Roche), and 20% glycerol] as previously described (Kanemaru et al., 2017). Nuclear extracts (5 μl) in microwells were used to evaluate NF-κB DNA-binding activity.

Histological analysis

Frozen 10-μm-thick mouse tumor tissue sections in Tissue-Tek OCT compound (Sakura Finetek, Torrance, CA, USA) or cells plated in chamber slides (Lab-Tek II Chamber Slide; Thermo Fisher Scientific) were fixed in 4% paraformaldehyde and blocked with 3% BSA in PBS. Formalin-fixed paraffin-embedded sections of primary tumor tissues (4 μm thick) from patients with no history of systemic treatment, including treatment with ICIs, were used for immunofluorescence analyses.

Immunofluorescent staining was performed using the following antibodies and reagents: anti-mouse EGR1 (ab174509, Abcam), anti-mouse EGR1 (ab133695, Abcam), anti-human EGR1 (ab194357, Abcam), Alexa Fluor 647-goat anti-rabbit IgG (H+L) (A-21245; Thermo Fisher Scientific), Alexa Fluor 405-goat anti-rabbit IgG H&L (Abcam), Hoechst 33342 solution (Dojindo, Kumamoto, Japan), APC anti-human CD20 Antibody (BioLegend), Alexa Fluor 594 anti-MART-1 antibody (BioLegend), APC anti-human CD56 (NCAM) antibody (BioLegend), APC anti-human CD68 antibody (BioLegend), and APC anti-human CD11c antibody (BioLegend). The dilution ratios for anti-EGR1 and Hoechst 33342 solution were 1:500 and 1:5000, respectively. The dilution ratios for other antibodies were 1:100. Images were obtained using a BZ-9000 (Keyence, Osaka, Japan), FV1200 (Olympus, Tokyo, Japan) or IN Cell Analyzer 2200 (GE Healthcare, Little Chalfont, UK). The cell-counting software Developer Toolbox of IN Cell Analyzer was used to determine the ratio of EGR1-positive cells to the total number of cells in whole tumor sections by counting EGR1-positive cells and cell nuclei (Tagawa et al., 2020).

Analysis of human specimens

Informed consent was obtained from the participant involved in the study. All procedures performed in studies were in accordance with the ethical standards of the institutional and/or national research committee and with the 1964 Helsinki Declaration and its later amendments or comparable ethical standards.

Tissue digestion for cell population analyses

Tissues were isolated from mice and placed in 10 mL of MEM containing 1 mg/mL collagenase type II (C6885; Sigma-Aldrich). Tissues were disrupted with surgical scissors and incubated at 37 °C for 30 min. Samples were filtered through 40-μm filters, and erythrocytes were removed by incubation for 3 min with ACK Lysing Buffer (Gibco, Life Technologies). After two washes with magnetic-activated cell sorting buffer (0.5% BSA and 2 mM EDTA in PBS, pH 7.2), samples were stained for analysis by flow cytometry, as previously described (Kanemaru et al., 2017). Leukocyte subpopulations were generally defined as follows: DCs, $CD45^+$ $CD11c^+$ cells; macrophages, $CD45^+$ $CD11b^+$ $F4/80^+$ cells; $CD4^+$ T cells, $CD45^+$ $CD3^+$ $CD4^+$ cells; $CD8^+$ T cells, $CD45^+$ $CD3^+$ $CD8^+$ cells; natural killer cells, $CD45^+$ $NK1.1^+$ cells; and B16-F1 tumor cells, $CD45^-$ melanoma $gp100^+$ cells.

Measurement of lactate concentration in tumors

The concentrations of lactate in tumors were measured as previously described (Maeda-Otsuka et al., 2019; Ohashi et al., 2017). Tumor specimens from mice were homogenized in PBS (1 μl per 1 mg tumor) and centrifuged. The concentrations of lactate in the obtained supernatants were measured using a Colorimetric Lactate Assay Kit (Cell Biolabs, San Diego, CA).

ChIP-seq analysis

ChIP analysis was performed using ChIP-IT Express Enzymatic (Active Motif) (Kanemaru et al., 2018). BMDCs (2×10^7) were stimulated with LPS (100 ng/ml) and lactate (20 mM). After 24 h, the cells were fixed with 20 ml of 1% formaldehyde for 10 min, followed by a wash with 10 ml of PBS, and the fixation reaction was stopped by adding 10 ml of glycine stop fix solution for 5 min. Cell extracts were prepared in lysis buffer and zhomogenized using a Dounce homogenizer (BioMasherII; Nippi, Tokyo, Japan) on ice. Enzymatic shearing to produce DNA fragments was performed for 30 min. Immunoprecipitation was then performed using 3 μg of anti-EGR1 (15F7) (Cell Signaling Technology) or anti-histone H3 (acetyl K27) (ab4729; Abcam). The samples were incubated overnight with 25 μl of protein G magnetic beads, and then the beads were washed. DNA was eluted in 50 μl of elution buffer, and 50 μl of reverse cross-linking buffer was added. Samples were centrifuged, and the resulting supernatants were collected and incubated at 95 °C for 15 min. After samples were returned to room temperature, RNase and proteinase K were added, and the samples were incubated for 1 h at 37 °C. DNA was then purified using the Chromatin IP DNA Purification Kit (58002; Active Motif) according to the manufacturer's instructions. ChIP-seq was performed by Filgen (Aichi, Japan), and the resulting data were analyzed by CLC Genomics Workbench 10 (Qiagen, Hilden, Germany).

The potential transcription factor–binding regions were estimated using TFBIND software (RIKEN, Yokohama, Japan) (Tsunoda and Takagi, 1999).

ChIP-PCR analysis

ChIP analysis was performed using ChIP-IT Express Enzymatic (Active Motif). RAW 264.7 cells (1.5×10^7) were transfected with 60 μg of plasmid encoding *Srf* using the Neon Transfection System (Thermo Fisher Scientific) at 1680 V for 20 msec. After 12 h, the cells were fixed with 1% formaldehyde for 10 min followed by a wash with PBS; the fixation reaction was stopped by adding glycine stop fix solution for 5 min. Cell extracts were prepared in lysis buffer and zhomogenized using a Dounce homogenizer (BioMasherII, Nippi) on ice. Enzymatic shearing was performed for 30 min, and DNA fragments were obtained (Input). Immunoprecipitation was performed using 3 μg of normal rat IgG (sc-2026; Santa Cruz Biotechnology) or rat anti-SRF antibody (2C5; Active Motif). Samples were incubated overnight with 25 μl of protein G magnetic beads, and then the beads were washed. DNA was eluted in 50 μl of elution buffer and 50 μl of reverse cross-linking buffer was added. The supernatants were then collected and incubated at 95 °C for 15 min. After samples were returned to room temperature, RNase and proteinase K was added, and the samples were incubated for 1 h at 37 °C. Input samples and precipitated DNA were analyzed by PCR using primers that detect sequences containing the SRF binding site of the *CD80* promoter: 5′-TGGCAGTCACTCTGTGTCCAG-3′ and 5′- CTAGTAAGAGTCTATTGAGG-3′.

Co-immunoprecipitation

Cells (1×10^6) were suspended in 100 μL of a solution (buffer R) containing 8 μg of Myc-tagged *Egr1* plasmid and 8 μg of *Srf* plasmid. Cells were electroporated using the Neon Transfection System (Thermo Fisher Scientific) at 1,680 V for 20 ms. Transfected cells were plated at 5×10^6 cells per dish. After 12 h, cell extracts were prepared using lysis buffer [10 mM Hepes-KOH, pH 7.8, 10 mM KCl, 0.1 mM EDTA, pH 8.0, protease inhibitor mixture (Roche), and 0.1% Nonidet P-40]. Lysates (50 μg) were incubated with 4 μg of normal rat IgG (sc-2026; Santa Cruz Biotechnology) or rat anti-SRF (2C5; Active Motif) in a total volume of 110 μL. The samples were incubated at 4 °C for 1 h on a tube rotator. Protein G-Sepharose (25 μL of 50% slurry; ab193259, Abcam) was added, and the mixture was agitated at 4 °C for 1 h. After centrifugation, the pellet was washed four times with TBS (50 mM Tris and 150 mM NaCl, pH 7.5). Samples were analyzed by standard SDS-PAGE immunoblotting using anti-c-Myc antibody (ab32072, Abcam) and anti-SRF antibody (ab53147, Abcam) from a different host species.

siRNA transfection

RAW 264.7 cells (1×10^6) were suspended in 100 μL of a solution (buffer R) containing 100 nM of *Gpr81* siRNAs, *Srf* siRNAs, or negative control siRNAs (Thermo Fisher Scientific). Cells were electroporated using the Neon Transfection System (Thermo Fisher Scientific) at 1,680 V for 20 ms. Transfected cells were plated at 5×10^6 cells per dish. After 24 h, cells were collected for experiments. Knockdown of the genes were confirmed by immunoblotting.

QUANTIFICATION AND STATISTICAL ANALYSIS

Database analysis

The results of database analysis shown here are in whole or part based upon data generated by TCGA Research Network: https://www.cancer.gov/tcga. Gene expression analysis was determined with the RNA-seq dataset acquired from skin cutaneous melanoma patients in TCGA data (TCGA-SKCM). Properties of patients selected here were filtered based on the following: sample type; primary tumor, site of resection; skin, stage; II and III, primary diagnosis; nodular melanoma, amelanotic melanoma, lentigo maligna melanoma, acral lentiginous melanoma, malignant melanoma (NOS).

Statistics

All statistical analyses were performed using GraphPad Prism software v8 (GraphPad, San Diego, CA, USA). A two-tailed Student's *t*-test or Welch's *t*-test was performed for the comparison of two independent normally distributed groups. Mann–Whitney's U test was used to compare two sets of non-normally distributed data. Pearson's correlation coefficient was used to evaluate the correlations. A *p*-value of less than 0.05 was considered statistically significant for all tests.